

Physical and Biological Controls on the Carbonate Chemistry of Coral Reef Waters: Effects of Metabolism, Wave Forcing, Sea Level, and Geomorphology

James L. Falter^{1,2,3*}, Ryan J. Lowe^{1,3}, Zhenlin Zhang^{1,2,3}, Malcolm McCulloch^{1,2,3}

1 School of Earth and Environment, University of Western Australia, Perth, Western Australia, Australia, **2** ARC Centre of Excellence for Coral Reef Studies, University of Western Australia, Perth, Western Australia, Australia, **3** The UWA Oceans Institute, University of Western Australia, Perth, Western Australia, Australia

Abstract

We present a three-dimensional hydrodynamic-biogeochemical model of a wave-driven coral-reef lagoon system using the circulation model ROMS (Regional Ocean Modeling System) coupled with the wave transformation model SWAN (Simulating WAVes Nearshore). Simulations were used to explore the sensitivity of water column carbonate chemistry across the reef system to variations in benthic reef metabolism, wave forcing, sea level, and system geomorphology. Our results show that changes in reef-water carbonate chemistry depend primarily on the ratio of benthic metabolism to the square root of the onshore wave energy flux as well as on the length and depth of the reef flat; however, they are only weakly dependent on channel geometry and the total frictional resistance of the reef system. Diurnal variations in $p\text{CO}_2$, pH, and aragonite saturation state (Ω_{ar}) are primarily dependent on changes in net production and are relatively insensitive to changes in net calcification; however, net changes in $p\text{CO}_2$, pH, and Ω_{ar} are more strongly influenced by net calcification when averaged over 24 hours. We also demonstrate that a relatively simple one-dimensional analytical model can provide a good description of the functional dependence of reef-water carbonate chemistry on benthic metabolism, wave forcing, sea level, reef flat morphology, and total system frictional resistance. Importantly, our results indicate that any long-term (weeks to months) net offsets in reef-water $p\text{CO}_2$ relative to offshore values should be modest for reef systems with narrow and/or deep lagoons. Thus, the long-term evolution of water column $p\text{CO}_2$ in many reef environments remains intimately connected to the regional-scale oceanography of offshore waters and hence directly influenced by rapid anthropogenically driven increases in $p\text{CO}_2$.

Citation: Falter JL, Lowe RJ, Zhang Z, McCulloch M (2013) Physical and Biological Controls on the Carbonate Chemistry of Coral Reef Waters: Effects of Metabolism, Wave Forcing, Sea Level, and Geomorphology. PLoS ONE 8(1): e53303. doi:10.1371/journal.pone.0053303

Editor: Inés Álvarez, University of Vigo, Spain

Received: July 25, 2012; **Accepted:** November 30, 2012; **Published:** January 9, 2013

Copyright: © 2013 Falter et al. This is an open-access article distributed under the terms of the Creative Commons Attribution License, which permits unrestricted use, distribution, and reproduction in any medium, provided the original author and source are credited.

Funding: Support for JLF and MM was provided by the Australian Research Council (ARC) Centre of Excellence for Coral Reef Studies. Support for RJL was provided by the ARC Future Fellows program. Support for ZZ was provided by the ARC Super Science Fellowship program. All use of supercomputing resources was supported through iVEC (<http://www.ivec.org/about-ivec>). The funders had no role in study design, data collection and analysis, decision to publish, or preparation of the manuscript.

Competing Interests: The authors have declared that no competing interests exist.

* E-mail: jim.falter@uwa.edu.au

Introduction

Rapidly rising levels of atmospheric CO_2 are expected to continue decreasing seawater pH and carbonate mineral saturation states across the world's oceans through a process commonly referred to as 'ocean acidification' [1–3]. Such trends have caused particular concern for the sustainability of coral reefs; ecosystems whose function and structure are ultimately dependent upon the biogenic precipitation of calcium carbonate [4–6]. Consequently, the sensitivity of calcification to changing carbonate chemistry has received considerable attention over the past decade. Much of this work has been carried out through manipulative experiments of live communities using aquaria or mesocosms where selected input variables can be carefully controlled [7–10]. The results of these studies have, however, demonstrated a wide range of variation depending not only on the calcifying species, but also on the experimental design [8,11]. A recent process-based synthesis [12] suggests that the impact of ocean acidification will be bi-modal: i.e., healthy calcifiers capable of pH up-regulation at the site of calcification (e.g., coral) demonstrate a high degree of resilience to

changes in ambient carbonate chemistry whereas those calcifiers lacking the ability to up-regulate pH (e.g., forams) appear far more sensitive to changes in ambient $p\text{CO}_2$. Thus, predicting the future response of reef calcifiers to changing atmospheric $p\text{CO}_2$ is still uncertain. Furthermore, there are additional interactive effects of increased $p\text{CO}_2$ on the ecology of reef biota that extend beyond rates of skeletal growth, yet these still remain poorly understood [13–16].

It has been well-known for many decades that shallow reef communities can alter the chemistry of their environment through their own metabolic activity [17–19]. For example, Smith 1973 [20] first demonstrated that the $p\text{CO}_2$ of reef waters are generally not in equilibrium with the atmosphere on short timescales, a direct outcome of community metabolism driving diurnal variations in water column carbonate chemistry (see Fig. 2 and Fig. 4 from that paper). Numerous subsequent studies have shown that the biological activity of reef communities can drive variations in $p\text{CO}_2$ that range from levels below a pre-industrial atmosphere (<285 μatm) to greater than predicted for the earth's atmosphere by the year 2100 under one of the most severe IPCC forecasts

(~1000 μatm [21], Table 1). Hence, distinguishing anthropogenically driven changes in water column carbonate chemistry from natural variations could be far more challenging in reef environments than in the open ocean [22]. These observations, combined with more recent experimental work, have also led to the suggestion that biologically driven changes in water column carbonate chemistry could be providing a natural feedback on rates of calcification [23]. Because of the potential importance of this hypothesis, recent field studies have begun to more carefully examine the relationship between rates of net community calcification and in situ carbonate chemistry versus other important variables such as light, temperature, net production, and nutrients [23–26].

Although there has been a recent renewed interest in how benthic reef metabolism alters the carbonate chemistry of coral reef waters [27–30], comparatively little attention has been given to the role that geomorphology and hydrodynamics play in modulating biologically driven changes in water chemistry. This is surprising since it is well-known that changes in water chemistry are as dependent on the residence time or ‘age’ of water masses as they are on the average rates of inorganic and biological reactions [31]. The residence time of reef waters change with location and time depending on the overall morphology of the reef system as well as on the hydrodynamic forcing mechanisms driving circulation [32,33]. Circulation in most shallow reef systems is predominantly wave-driven (depending upon exposure), but it is also influenced by the tides and in some cases wind [33–35]. While some assessment of local hydrodynamics has always been critical for estimating in situ rates of benthic community metabolism, in many instances precise measurements of water chemistry are combined with only very rough estimates of flow speed, direction, and/or water residence time. This makes it difficult to properly assess the true uncertainty in derived rates of benthic metabolism (e.g., net production and net calcification).

Field studies of reef water chemistry and derived rates of benthic community metabolism are thus complicated by ever-changing circulation patterns and water residence times. The application of numerical hydrodynamic models within coral reef systems has provided us with one means to overcome this limitation [34–36]. These models essentially divide an entire reef system into many grid cells (~ 10^5 to 10^6) that act as individual ‘control volumes’ through which net inputs and outputs of mass and momentum are

budgeted. More recently, the inclusion of benthic metabolism within such models have provided the additional means for modeling spatial and temporal changes in nutrient concentrations and carbonate chemistry within coral reef systems [33,37]. The application of coupled hydrodynamic-biogeochemical models has thus provided us with a powerful new tool for studying oceanic and atmospheric forcing of reef biogeochemical cycles.

While prior efforts have used numerical models for the study of specific reef systems, the range of biogeochemical changes that an individual reef system can exhibit is still constrained by its particular geomorphology, benthic composition, and by the specific oceanic and atmospheric conditions driving internal circulation and exchange with offshore waters. This constrained range of observable behavior is often further limited by the finite duration of many field studies (generally weeks or less). Long-term monitoring efforts can overcome some of these time-dependent limitations, but such programs generally come at great cost and are therefore limited in number. To overcome the limitation of examining a single reef system under pre-defined conditions, we developed a flexible model reef system with simple but representative geomorphologies and rates of benthic metabolism that can be subject to a wide range of hydrodynamic forcing. We show that this approach offers the same level of focus and control in system-scale studies that experimental mesocosms accomplish in organism-scale studies. Both approaches complement more realistic but less-controlled field studies by exploring the effects of specific forcing variables on the response of a system (or organism) over a broader range of controlled conditions. If designed properly, the hydrodynamics and biogeochemistry of these experimental idealized reefs can be remarkably similar to real reef systems [37,38].

The present study is aimed at exploring how hydrodynamic factors (wave forcing and sea level), benthic metabolism, and reef geomorphology act in combination to fundamentally influence water column carbonate chemistry across representative wave-driven reef systems under a realistic range of input variables. The wealth of data on benthic net production, benthic net calcification, wave transformations, circulation, and morphology already available in the literature provide us with ample means to constrain our model domain within realistic limits (Tables 2 and 3). In this paper we first develop a set of relatively simple analytical equations to describe how changes in water column carbonate chemistry functionally depend on rates of benthic metabolism, wave forcing, sea level, and geomorphology using a simplified one-dimensional framework. Second, we simulate changes in wave heights, currents, and carbonate chemistry across a fully three-dimensional wave-driven reef-lagoon system under a wide range of physical and biogeochemical conditions. Third, we test the ability of the simple analytical model to replicate the behavior of our fully three-dimensional numerical model as well as to predict the variations in water column $p\text{CO}_2$ that have been observed in natural reef systems. Finally, we discuss the utility of our simplified model to simulate larger reef systems as well as its implications for future studies of ocean acidification in coral reef systems.

Background

Prior studies of reef metabolism and wave driven circulation. In a seminal review of reef community carbon metabolism, Kinsey 1985 [39] found that rates of daily benthic community gross production (P), respiration (R), and net calcification (G_{net}) for entire reef flats tended to cluster around typical or ‘standard’ values of 580, 580, and 110 $\text{mmol C m}^{-2} \text{d}^{-1}$, respectively. These rates were found to be largely independent of latitude and longitude (at least across the Indo-Pacific) despite seasonal and spatial variations in light, ocean sea surface

Table 1. Observed ranges in the $p\text{CO}_2$ of reef waters worldwide (μatm).

Site	min	max	Ref.
Enewetak, Marshall Islands	150	320	[20]
Siraho Reef, Ishigaki, Ryukyus	160	520	[88]
Tiahura Reef, Moorea, Fr. Polynesia	240	420	[57]
Yonge Reef, north GBR	250	700	[57]
Bora Bay, Miyako, Ryukyus	200	550	[56]
Rukan-Sho, Okinawa, Ryukyus	40	900	[89]
Grand Bahama Bank, Bahamas	300	380	[28]
Hog Reef, Bermuda	320	560	[23]
Kaneohe Bay, Oahu, Hawaii	250	680	[25]
Lady Elliot Island, south GBR	100	1300	[30]
Sandy Bay, Ningaloo, W. Australia	220	440	[24]

doi:10.1371/journal.pone.0053303.t001

Table 2. Daily rates of reef carbon metabolism worldwide.

Site	<i>P</i>	<i>R</i>	<i>G_{net}</i>	<i>P:R</i>	<i>G_{net}:P</i>	Ref.
Rongelap Atoll, French Polynesia	330	290	-	1.14	-	[19]
Enewetak Atoll, Marshall Islands	830	830	110	1.00	0.13	[18,20,90]
Fringing reef, Kauai, Hawaii	660	630	-	1.05	-	[17]
Laccadives, Northern Indian Ocean	520	210	-	2.48	-	[91]
One Tree Island, Central GBR	610	590	130	1.03	0.21	[92–94]
Guam, Marianas Islands	600	550	-	1.09	-	[95]
Lizard Island, Northern GBR	620	610	110	1.02	0.18	[96,97]
French Frigate Shoals, NWHI	540	330	180	1.64	0.33	[98]
Rib Reef, Central GBR	600	670	100	0.90	0.17	[99]
Tulear, Madagascar	1580	920	50	1.72	0.03	[100]
Tiahura Reef, Moorea, Fr. Polynesia	660	610	170	1.15	0.26	[101,102]
Yonge Reef, Northern GBR	1280	1250	250	1.02	0.20	[101]
Soraho, Ishigaki Island, Ryukyus	150	100	20	1.50	0.13	[88]
Bora Bay, Miyako Island, Ryukyus	720	530	50	1.36	0.07	[56,103]
St. Gilles Reef, La Reunion Island	640	660	160	0.97	0.25	[104]
St. Leu Reef, La Reunion Island	1540	1280	150	1.20	0.10	[104]
Nature Reserve Reef, Gulf of Aqaba	340	300	50	1.13	0.15	[26,105]
Kaneohe Bay barrier reef, Hawaii	670	590	250	1.17	0.36	[25,44,45]
Sandy Bay, Ningaloo, W. Australia	1230	1190	200	1.03	0.16	[24]
Coral Bay, Ningaloo, W. Australia	-	-	120	-	-	[33]
Mean	740	640	130	1.24	0.18	
<i>Std. Dev.</i>	390	340	70	0.38	0.09	
<i>Std. Err.</i>	90	80	20	0.09	0.02	
Median	640	610	130	1.09	0.17	
Model Central Case	660	610	130	1.08	0.20	<i>This study</i>

Daily integrated rates of community production (*P*), respiration (*R*), and net calcification (*G_{net}*) published for reef flat communities across the Indo-Pacific over the last 60+ years. Also shown are the ratios of production to respiration and production to net calcification. Data presented for systems from which there were multiple sources were averaged. ‘-’ means no data available. Data for Rongelap through Tulear were taken from Kinsey 1985 [39]. doi:10.1371/journal.pone.0053303.t002

temperature, and carbonate mineral saturation state; although seasonality in *G_{net}* appeared to be stronger in higher-latitude reefs [39]. More recent data collected over the 30 years following the Kinsey 1985 review has not fundamentally changed this general assessment of reef flat metabolism (Table 2). However, a review of the larger cumulative data set indicates that 1) rates of benthic reef carbon metabolism fall within a range that is a factor of two lower or higher than the ‘standard’ or median rates (*P* ≈ 300 to 1200 vs.

640 mmol C m⁻² d⁻¹ and *G_{net}* ≈ 50 to 250 vs. 130 mmol C m⁻² d⁻¹, Table 2), and 2) shallow reef communities are modestly net autotrophic on average (i.e., *P:R* ~ 1.1, Table 2).

Although there have been fewer studies of wave transformations and/or wave-driven circulation across shallow reef systems, it is nonetheless clear that the geomorphology and hydrodynamic forcing of many reef systems also fall within well-defined ranges (Table 3). The archetypal or ‘standard’ reef (Fig. 1) has a reef flat that is ~500 m long (*L_r*) and ~1 m deep at mean sea level (*h_r*), is backed by a lagoon that is anywhere from 500 m to ~20 km long (*L_{lag}*), has channels that are 10% to 20% the width of the reef flat (*W_c^{* ≡ *W_c*/*W_r*) and 2 to ~20 m deep (*h_c*), and is exposed to offshore significant wave heights of between 1 and 2 m (*H₀*). As a result, cross-reef flow speeds (*U_r*) are generally between 0.1 to 0.2 m s⁻¹ resulting in cross-reef transports (*q_r*) that are between 0.1 and 0.2 m² s⁻¹ (*q_r* = *U_r* × *h_r*).}*

Theory. Lowe et al. 2009 [40] showed that a simple one-dimensional (cross-reef) model captures the essential dynamics of wave-driven circulation in shallow coastal reef systems (i.e., forcing and response) despite the more complex, two-dimensional (horizontal) structure in the circulation exhibited by real reef systems [34]. Circulation in wave-exposed reef systems is ultimately controlled by wave breaking in the shallow surf zone which, in turn, causes the mean sea level at the reef crest to increase relative to offshore. This wave setup height (*η*) in turn drives the flow of water across the shallow reef flat, through the lagoon, and out the nearest channel (Fig. 1). Gourlay and Colleter 2005 [41] developed a semi-empirical formulation to describe the maximum wave setup at the reef crest (*η_{crest}*) as a function of incident wave power which can be approximated by the following relationship:

$$\eta_{\text{crest}} = \frac{3K_p\sqrt{g}}{64\pi} \cdot \frac{H_0^2 T}{d_r^{3/2}} \quad (1)$$

where *K_p* is the empirical reef profile factor that depends on the reef slope (~0.8 for a near-vertical reef face, *H₀* is the offshore wave height, *T* is the wave period, *d_r* is the total depth of the reef flat equal to the sum of the reef flat depth at mean sea level and the reef flat setup (*d_r* = *h_r* + *η*), and *g* is the gravitational acceleration constant (see Appendix S1). The *H₀²T* term in the second numerator is proportional to the shoreward flux of surface wave energy [42].

Bottom friction causes setup to decrease across the reef flat and channel such that

$$\eta_{\text{crest}} = \Delta\eta_{\text{reef}} + \Delta\eta_{\text{channel}} \quad (2)$$

assuming offshore mean sea level is zero (*η_{off}* = 0). Because flow speeds in the channel are generally higher than on the reef flat, reef channels can potentially provide enough frictional resistance to the wave-driven flow such that setup in the lagoon becomes a significant fraction of the setup at the reef crest [40,43]. Assuming a balance of both mass and momentum across the reef and channel, we can derive an expression for the cross-reef transport as a function of the offshore wave conditions and the combined morphology of the reef flat and channels:

$$q_r = K' \left(\frac{H_0^2 T}{h_r^2 L_r} \right)^{1/2} \left(\frac{\bar{f}_r}{2h_r^3} + \frac{\bar{f}_c}{2h_c^3 W_c^{*2}} \right)^{-1/2} \quad (3)$$

Table 3. Offshore wave heights, transport, and geomorphology of reefs worldwide.

Site	H_o	U_r	q_r	h_r	L_r	W_r	h_c	L_{lag}	W_c^*	Refs
Kaneohe Bay, Oahu, Hawaii	2.0	0.13	0.26	2.0	1500	5500	8	1000	0.15	[106] [40]
Sandy Bay, Ningaloo Reef	1.5	0.10	0.13	1.3	450	3000	4	500	0.18	[37] [35]
Coral Bay, Ningaloo Reef	2.0	0.20	0.20	1.0	500	1100	5	700	0.15	[33]
Moorea, French Polynesia	1.5	0.18	0.31	1.7	450	3750	10 ^a	500	0.05	[107] [43]
Bora Bay, Miyako, Ryukyus	1.0	0.25	0.25	1.0	250	600	2	500	0.15	[51]
Heron Island, South GBR	3.5	–	–	2.0	700	8000	3	1000	0.20	[41]
John Brewer Reef, Central GBR	0.3	0.08	0.08	1.0	400	5000	8	2000	0.10	[108]
Rib Reef, Central GBR	–	0.15	0.15	1.0	400	500	10	500	0.30	[109] [99]
Yonge Reef, North GBR	2.0	–	–	0.8	500	5800	35 ^c	–	0.25	[110]
Abore Reef, New Caledonia	1.0	0.20	0.16	0.8	150	24000 ^b	18 ^b	20000 ^b	0.10	[111]
Mean	1.6	0.16	0.19	1.3	530	3700	6.3	840	0.16	
Std. Dev.	0.9	0.06	0.08	0.5	380	2600	9.8	500	0.07	
Std. Err.	0.3	0.02	0.03	0.1	120	900	3.5	200	0.02	
Median	1.5	0.17	0.18	1.0	450	3800	6.5	600	0.15	
Model Central Case	1.5	0.18	0.18	1.0	500	4000	6.0	700	0.15	<i>This study</i>

Summary of offshore wave heights, flow, and reef morphology parameters reported from hydrodynamic studies of reefs across the Indo-Pacific and augmented by the additional analysis of satellite imagery provided by Google Earth. Notes: (a) the effective channel depth for Moorea was set at 10 m to reflect that setup in the channel was roughly one-half of that at the reef crest even though maximum channel depths can exceed 30 m [43], (b) the reef flat width, depth of channel, and lagoon width for Abore Reef were considered extreme and excluded from the calculation of the group statistics, (c) the extreme depth of the channel adjacent to Yonge Reef is relevant to exchange for an entire section of the north GBR lagoon, not just local flow across Yonge Reef and therefore excluded from the calculation of the group statistics (see Discussion). See Background, Fig. 1, or Table 4 for additional description of variables shown.
doi:10.1371/journal.pone.0053303.t003

where K'_p is equal to $\left(3K_p g^{3/2} / 64\pi\right)^{1/2}$, and \bar{f}_r and \bar{f}_c are the bottom friction coefficients corresponding to the depth-averaged flow speed over the reef flat and in the channel, respectively (see Appendix S2). \bar{f}_r and \bar{f}_c are primarily a function of physical bottom roughness expressed in terms of a hydraulic roughness length scale z_0 and the local water depth, but are also subject to wave-current interactions; especially within the wave-exposed channel (see Appendix S3).

Assuming a vertically well-mixed water column, the change in concentration of a reactive species with space ($\partial C / \partial s$) and time ($\partial C / \partial t$) along a flow streamline (\vec{s}) is primarily a function of the benthic flux (J), the water depth, and the horizontal transport

$$J = h \frac{\partial C}{\partial t} + q \frac{\partial C}{\partial s} \quad (4)$$

Prior studies have shown that the advective term (second term, right-hand side) is generally much greater than the time-dependent term (first term, right-hand side) for water crossing the reef flat [24,44,45].

$$J_r \approx q \frac{\Delta C}{\Delta s} \quad (5)$$

Thus, we can re-formulate the change in reactive species concentration across the reef flat (ΔC_r) as a function of the reef flat length ($\Delta s = L_r$) and the cross-reef transport, i.e.

$$\Delta C_r = \frac{J_r}{q_r} L_r \quad (6)$$

Combining Eq. 3 and Eq. 6 we get the following relationship

describing the change in reactive species concentration across the reef flat as a function of the benthic flux, incident wave forcing, reef morphology, and frictional roughness:

$$\Delta C_r = \frac{1}{K'_p} \left(\frac{J_r}{H_0 \sqrt{T}} \right) \left(\frac{L_r^2}{h_r} \right)^{3/4} \left(\bar{f}_r + \frac{\bar{f}_c}{h_c^* W_c^{*2}} \right)^{1/2} \quad (7)$$

where h_c^* is the ratio of the channel depth to the reef flat depth ($h_c^* \equiv h_c / h_r$) and all other variables are defined as before. Eq. 7 can be expressed more simply as:

$$\Delta C_r = \frac{1}{K'_p} J'_r L_r'^{3/4} \sqrt{\bar{f}_{sys}} \quad (8)$$

where

$$\begin{aligned} J'_r &\equiv \frac{J_r}{H_0 \sqrt{T}} \\ L'_r &\equiv \frac{L_r^2}{h_r} \\ \bar{f}_{sys} &\equiv \bar{f}_r + \frac{\bar{f}_c}{h_c^* W_c^{*2}} \end{aligned} \quad (9)$$

Eq. 8 indicates that changes in the concentration of a reactive species depend on three fundamental properties: 1) a forcing factor determined by the ratio of benthic metabolism or bottom flux to the square root of the onshore wave energy flux (J'_r), 2) a reef flat geometry factor determined by the length and depth of the reef flat (L'_r), and 3) the total resistance of the reef system to wave-driven

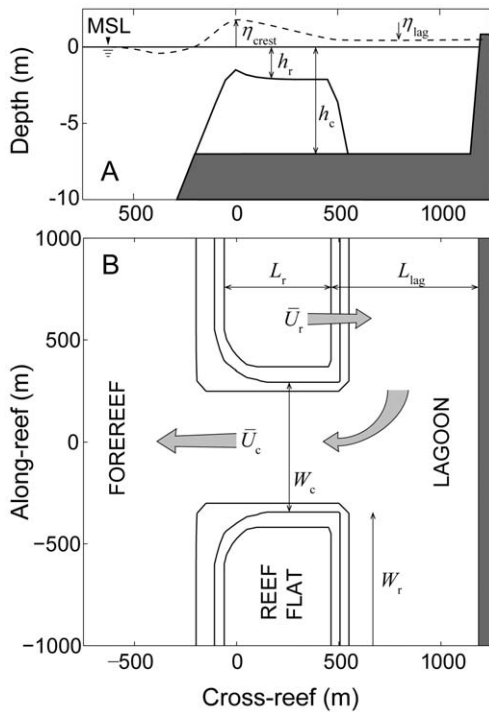


Figure 1. Schematics of the coastal reef-lagoon system. (A) side-view depth profile of the reef flat and (B) top-view of part of the domain containing sections the forereef, reef flat, lagoon and channel. The ratio of vertical to horizontal scale in (A) is 75:1. The main reef structures in (B) are outlined by the 1.5-m, 3-m, and 6-m isobaths. Dark grey regions represent land or solid reef basement. Light grey arrows represent the general direction of wave-driven circulation. The reference origin set at the intersection of the reef crest line and mid-channel is provided only to illustrate the scale of the reef features. All morphological dimensions shown reflect those of the central model case; however, an extra +1 m of sea level has been added to (A) to better illustrate profiles of reef flat depth and cross-reef setup. See Background and Table 4 for additional description of all variables shown.
doi:10.1371/journal.pone.0053303.g001

flow (\bar{f}_{sys}). The role of each of these factors can be explained as follows. Greater bottom fluxes will drive greater changes in water chemistry while stronger wave forcing will increase transport and decrease the contact time of water with the reactive benthos thus reducing changes in concentration. The length and depth of the reef flat are important for several reasons. Firstly, changes in water chemistry from variable bottom fluxes become increasingly diluted as the depth of the water column increases. Secondly, the longer the reef flat, the greater the time for water to interact with the reef (Eq. 6). Thirdly, as the length of the reef flat increases, the cross-reef gradient in setup across the reef becomes weaker ($\Delta\eta/\Delta x$), and cross-reef transport decreases (Eq. 3); thus, increasing the change in concentration per unit length of reef flat (Eq. 6). Fourthly, the greater the reef flat depth, the lower the maximum setup at the reef crest (Eq. 1), and the weaker the cross-reef transport; a result which also increases the change in concentration per unit length of reef flat (Eq. 6). The total frictional resistance of the reef system controls the rate of volume transport through the reef system under a given set of wave conditions. It is not only a function of the frictional roughness of the reef flat and channels, but also a function of the ratios of the channel depth to reef depth and the channel width to reef width as well. As the relative depth and/or width of the channel decrease (h_c^* or W_c^*),

the frictional resistance generated in the channels can become a significant impediment to overall wave-driven circulation. This results in longer water residence times and consequently larger changes in water chemistry (Eq. 7).

Methods

We define a central model case based on median and average rates of benthic metabolism, morphological dimensions, and wave forcing reported in the literature (see Tables 2 and 3). We assume that hourly rates of gross primary production, respiration, and net calcification are constant to some finite depth, and then decrease exponentially with depth proportional to the attenuation of light [33,46]. Next, we explore the sensitivity of the idealized reef hydrodynamic-biogeochemical model to changes in 1) the ratio of benthic metabolism to wave forcing, 2) the geometry of the reef flat, 3) the depth and width of the channels connecting the lagoon and ocean via their impact on total system frictional resistance, and 4) sea level. Exploring the influence of each of these factors often involves more than one variable (Table 4). In all model simulations (except two) we varied only one of the ten possible input variables choosing a perturbation-response approach to evaluating model sensitivity in order to keep the number of simulations tractable and to simplify the analysis of our results. These individual variables included H_0 , P , G_{net} , P_{lag} , h_r , L_r , L_{lag} , h_c , W_c , and the offshore sea level (η_{sea}).

Numerical Model

The hydrodynamic and biogeochemical processes were simulated using the three-dimensional ocean circulation model ROMS (Regional Ocean Modeling System, version 3.3) [47] two-way coupled to a spectral wave model SWAN (Simulating WAVes Nearshore, version 40.51) [48], based on recent nearshore routines implemented in ROMS [49]. The water column is divided into 4 vertical layers. A higher vertical resolution is not needed as the water column in the shallow reef area is assumed to be well-mixed [37]. A southward offshore boundary current of 0.25 m s^{-1} is chosen to simulate offshore momentum boundary conditions similar to those both observed and used in prior modeling studies [32,36]; however, subsequent simulations indicated that model results were not sensitive to the offshore current speed (see Tables S1 through S5). The less important processes of local wind wave generation, nonlinear wave-wave interaction, wave-current refraction, and dissipation due to white capping in SWAN were turned off [34]. Directional wave spectra were prescribed at the western (offshore) boundary as well as the offshore section of the northern and southern boundaries using time-varying significant wave heights, peak wave periods and peak wave directions, by assuming a standard JONSWAP (Joint North Sea Wave Project) frequency distribution, ($\gamma_f = 3.3$, $\sigma_a = 0.07$, $\sigma_b = 0.09$) and a cosine to the power 5 directional distribution. The wave direction is from the west (270°) in all simulations. Depth-limited wave breaking was modeled with a breaking coefficient of $\gamma = 0.7$, a value typically used in reef systems [34,50,51]. While there are three commonly used bottom boundary models to calculate wave-current interaction within ROMS, the Soulsby 1995 [52] model was chosen as it is computationally more efficient under a wide range of wave and current flow combinations and yet no less accurate than other models [37]. All model simulations were conducted in parallel using Message Passing Interface (MPI) on a supercomputer (iVEC; <http://ivec.org.au/>) using 132 processors.

The model domain consisted of one complete shallow reef flat bounded by a channel and one-half a reef flat to the north and to the south with a lagoon to the east (Fig. 2a) based on the design of

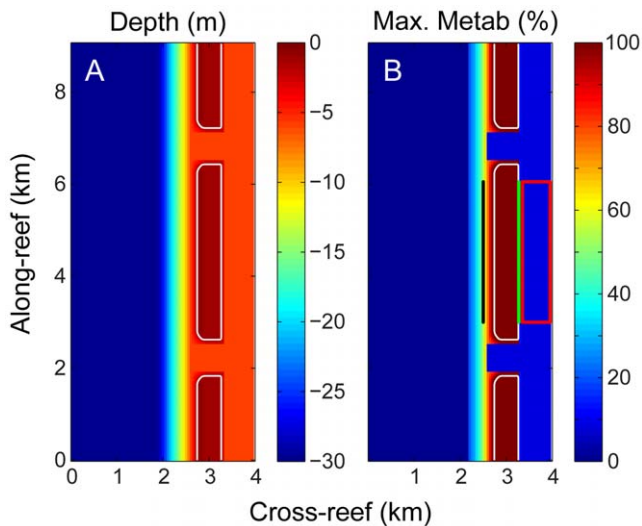


Figure 2. Bathymetry and benthic metabolism for the central model case. (A) Bathymetry and (B) rate of hourly metabolism (p , r , g_{net}) as a percentage of the maximum rate for the entire reef system. In panel B the forereef and backreef transects defined in later analyses are indicated by the heavy black and green lines, respectively; while the lagoon zone defined in later analyses is indicated by the red box. The values shown along the x and y axes are only to illustrate the scale of the model domain.

doi:10.1371/journal.pone.0053303.g002

Lowe et al. 2010 [38]. All model reefs reached a minimum depth of 0.5 m at the reef crest and then declined exponentially toward the back such that the average depth across the reef flat was equal to the target reef flat depth of h_r and the depth of the lagoon was always set equal to the depth of the channel h_c (Table 4, Fig. 1a). The combined widths of the reef flat and channels were kept constant and equal to 4600 m for all simulations. This means that as the channel width W_c increased, the reef width W_r decreased such that $W_r + W_c$ was equal to 4600 m in all simulations (Fig. 1b). This resulted in a model domain which was ~ 9 km long in the along-reef (north-south) direction and ~ 4 km in the cross-reef (east-west) direction (Fig. 2a). We needed a relatively small spatial resolution (50 m) to properly resolve changes in wave height, setup, and currents across the shallow forereef and reef flat [33,35,40]. Thus, to keep the model simple and tractable, we limited our simulations to lagoons that were 1500 m long (L_r) or less. The forereef slope was kept constant and equal to 1:30 for all simulations; a value we chose to be intermediate between steep-faced reefs (1:20 [41]) and more gently sloped reef fronts (1:40 [40]). The maximum depth of the domain was limited to 30 m, since prior work has shown that chemical reactions at these depths in the presence of an alongshore current have a negligible influence on changes on water column chemistry across coastal reef-lagoon systems [33]. Finally, a roughness length scale (z_0) of 0.03 m was chosen to represent the reef flat and forereef and 0.015 m for the lagoon to reproduce quadratic bottom drag coefficients similar to those observed in prior studies (0.01 to 0.03 [33,35,40]).

Biogeochemical Forcing

Hourly rates of gross production (p) and net calcification (g_{net}) were constrained to equal daily integrated rates over a 24-hour period:

$$P \equiv \int_0^{24} p(t) dt \quad (10)$$

$$G_{\text{net}} \equiv \int_0^{24} g_{\text{net}}(t) dt$$

(see Appendix S4). Hourly rates of respiration were assumed to be constant throughout the day

$$r = \frac{R}{24} = \frac{P}{(P : R)} \cdot \frac{1}{24} \quad (11)$$

Finally, hourly rates of net community production (np) were calculated as the difference between $p(t)$ and r

$$np(t) = p(t) - r \quad (12)$$

For the central model case we further assumed that the bottom of the lagoon and channels were comprised of sand communities whose daily gross production, respiration, and net calcification were 80, 70, and 20 $\text{mmol C m}^{-2} \text{d}^{-1}$, respectively [39,53–55]; however, we ran additional simulations to examine the effect of higher rates of lagoon metabolism on changes in carbonate chemistry ($P_{\text{lag}} = 330 \text{ mmol C m}^{-2} \text{d}^{-1}$ and $h_c = 3$ and 6 m, [39,56]).

Local benthic fluxes of Total Alkalinity (TA) and Dissolved Inorganic Carbon (DIC) were then calculated from hourly rates of g_{net} and np as

$$J_{\text{TA}} = -2g_{\text{net}} \quad (13)$$

$$J_{\text{DIC}} = -np - g_{\text{net}} \quad (14)$$

where negative fluxes represent net removal of TA or DIC from the water column [20]. Given that the residence times of waters within the reef flat, lagoon, and channel were always less than 24 hours in all simulations, that water column $p\text{CO}_2$ varied between undersaturated and oversaturated conditions with respect to the atmosphere over a diurnal cycle, and that air-sea CO_2 fluxes are generally very small relative to the combined influence of benthic net production and calcification ($< 1\%$ [20,57]); we ignored the air-sea exchange of CO_2 in the present model as it would have a negligible effect on simulated changes in carbonate chemistry on these time scales (~ 1 day or less).

Offshore waters were assumed to be at a uniform temperature of 25°C and salinity of 35, in equilibrium with the atmosphere ($p\text{CO}_2 = 390 \mu\text{atm}$), and having a sea surface TA typical of tropical surface waters worldwide ($2300 \mu\text{eq kg}^{-1}$ [58]). Offshore DIC and all other carbonate chemistry parameters were calculated from these defined input conditions using the CO2SYS program [59] based on pre-defined dissociation and solubility constants [60–63]. Preliminary simulations indicated that differences in the model predicted transport and carbonate chemistry parameters simulated on a 50-m resolution grid and those simulated on a 25-m resolution grid differed by less than a few percent; therefore, all subsequent simulations were run on a 50-m grid. Preliminary simulations also indicated that changes in carbonate chemistry across the domain reached equilibrium to within less than

Table 4. Variables and constants used in this paper.

Variable	Units	Description
P	$\text{mmol C m}^{-2} \text{ d}^{-1}$	Daily reef gross primary production
P_{lag}	$\text{mmol C m}^{-2} \text{ d}^{-1}$	Daily lagoon gross primary production
R	$\text{mmol C m}^{-2} \text{ d}^{-1}$	Daily reef respiration
G_{net}	$\text{mmol C m}^{-2} \text{ d}^{-1}$	Daily reef net calcification
p	$\text{mmol C m}^{-2} \text{ hr}^{-1}$	Hourly gross primary production
p_{max}	$\text{mmol C m}^{-2} \text{ hr}^{-1}$	Maximum hourly gross primary production
r	$\text{mmol C m}^{-2} \text{ hr}^{-1}$	Hourly respiration
np	$\text{mmol C m}^{-2} \text{ hr}^{-1}$	Hourly net production
g_{net}	$\text{mmol C m}^{-2} \text{ hr}^{-1}$	Hourly net calcification
d_{sed}	$\text{mmol C m}^{-2} \text{ hr}^{-1}$	Sediment dissolution rate
TA	$\mu\text{eq kg}^{-1}$	Total Alkalinity
DIC	$\mu\text{mol kg}^{-1}$	Dissolved Inorganic Carbon
$p\text{CO}_2$	μatm	Partial pressure of dissolved carbon dioxide
Ω	–	Carbonate mineral saturation state (calcite or aragonite)
Ψ	–	Molar ratio of CO_2 released from calcification
E_{d}	$\mu\text{mol m}^{-2} \text{ s}^{-1}$	Instantaneous downwelling planar PAR irradiance
$E_{\text{d,max}}$	$\mu\text{mol m}^{-2} \text{ s}^{-1}$	Maximum downwelling planar PAR irradiance
t_{sr}	hr	Time of sunrise
t_{ss}	hr	Time of sunset
k_{d}	m^{-1}	Light attenuation coefficient
h_{m0}	m	Depth of constant metabolism
H_0	m	Offshore significant wave height
T	s	Offshore peak wave period
K_{p}	–	Wave power transmission parameter
K'_{p}	–	Modified wave power transmission parameter
z_0	m	Roughness length scale
η_{crest}	cm	Wave setup at the reef crest
η_{lag}	cm	Wave setup in the lagoon
η_{sealvl}	cm	Added sea level above mean sea level
d_{r}	m	Reef flat depth (including waves and tides)
h_{r}	m	Reef flat depth at mean sea level
\bar{U}_{r}	m s^{-1}	Depth-averaged current
q_{r}	$\text{m}^2 \text{ s}^{-1}$	Depth integrated cross-reef transport
L_{r}	m	Reef flat length
W_{r}	m	Reef flat width
L_{lag}	m	Lagoon length
h_{lag}	m	Lagoon depth
τ_{lag}	hr, d	Lagoon residence time
h_{c}	m	Channel depth
h_{c}^*	–	Relative channel depth
\bar{U}_{c}	m s^{-1}	Depth-averaged channel current
q_{c}	$\text{m}^2 \text{ s}^{-1}$	Depth-integrated channel transport
W_{c}	m	Channel width
W_{c}^*	–	Relative channel width
\bar{f}_{r}	–	Depth-averaged reef flat current drag coefficient
\bar{f}_{c}	–	Depth-averaged channel current drag coefficient
\bar{f}_{sys}	–	Total reef system frictional resistance
J_{r}	$\text{mmol m}^{-2} \text{ hr}^{-1}$	Rate of benthic reef flat metabolism

Table 4. Cont.

Variable	Units	Description
J_r'	$\text{mmol m}^{-3} \text{hr}^{-1.5}$	Ratio of reef flat metabolic forcing to wave forcing
L_r'	m	Reef flat geometry factor

'-' represent dimensionless variables.

doi:10.1371/journal.pone.0053303.t004

$\sim 2 \mu\text{eq kg}^{-1} \text{d}^{-1}$ of TA, $\sim 1 \mu\text{mol kg}^{-1} \text{d}^{-1}$ of DIC, and less than $\sim 3 \mu\text{atm d}^{-1}$ of $p\text{CO}_2$ after the first 24 hours of simulation time. Therefore, all simulations were run for 2 days (simulation time) in order for diurnal changes in water column carbonate chemistry to reach an approximate steady state ($\partial C/\partial t < 1\% \text{d}^{-1}$) under the imposed constant hydrodynamic and forcing and diurnal variations in benthic metabolism.

Results

Three-dimensional simulations

Wave heights decreased rapidly near the reef crest due to depth-limited breaking with some wave energy penetrating into the deeper channels (Fig. 3b). This pattern of wave dissipation led to maximum wave-induced setup near the shallow reef crest. Wave setup then declined sharply across the reef flat before reaching levels within the lagoon that were less than on the reef flat, but still higher than offshore (Fig. 3c). The resulting spatial distribution of the wave setup drove a general pattern of circulation whereby waters moved lagoonward across the reef flat and seaward out the channels; a pattern consistent with numerous prior observations of wave-driven circulation in coral reefs [33–35,40,43,64]. Water flowing out of the main channels was quickly entrained by the southward alongshore current within $\sim 1 \text{ km}$ offshore of the channel entrance (Fig. 3d). For reference, the exact output of key hydrodynamic variables ($\eta_{\text{crest}}, q_r, \bar{U}_r, \eta_{\text{lag}}, q_c, \bar{U}_c$, and average significant wave heights in the channel H_c) for each of the 33 simulations are provided in Table 5.

Changes in TA, DIC, $p\text{CO}_2$, and Ω_{ar} across the reef flat at mid-day (i.e., peak solar irradiance) are driven by their benthic uptake from net production and net calcification; behavior consistent with numerous observations reported in the literature (Fig. 4). Water in the lagoon and channels exhibited both high and low ΔTA , ΔDIC , $\Delta p\text{CO}_2$, and Ω_{ar} due to the confluence of water masses which had traversed the shallow reef flat at different phases of day and night. This general spatial pattern was similar for all carbonate chemistry parameters differing only in scale and sign (negative for ΔTA , ΔDIC , $\Delta p\text{CO}_2$, and positive for ΔpH and $\Delta\Omega_{\text{ar}}$). Therefore, in the interest of economy, most of the results and discussion that follows will focus on variations in $p\text{CO}_2$ since this is the primary variable of interest with regards to future changes in atmospheric composition. Nonetheless, time-elapsd movies demonstrating hourly changes in ΔTA , ΔDIC , $\Delta p\text{CO}_2$, ΔpH and $\Delta\Omega$ across the entire reef domain over a 24-hr period are also provided (see Movies S1 through S5).

Diurnal changes in $\Delta p\text{CO}_2$ on the forereef appeared to follow quasi-sinusoidal variations (Fig. 5a), whereas diurnal variations in $\Delta p\text{CO}_2$ on the reef flat and in the lagoon exhibited more complex temporal behavior (Fig. 5b, 5c). This was largely due to the re-entrainment of channel outflow water into the cross-reef flow after exiting the channels and then moving southward across the forereef with the predominant alongshore current (Figs. 3d, 4, 5). Consequently, re-entrained low- $\Delta p\text{CO}_2$ water produced during

the day damped maximum nighttime values resulting in truncated or 'scalloped' maxima. This same pattern was evident in the time series of ΔTA and ΔDIC (not shown). It is possible that this effect could be even more pronounced when alongshore currents, including the associated horizontal mixing, on the forereef are particularly weak. However, reducing the magnitude of the offshore current by one-half relative to the central case had only a modest effect on diurnal profiles of forereef water column carbonate chemistry. Furthermore, prior field observations (not shown) suggest that our reef-scale models if anything slightly overestimate the observed variability in the chemistry of forereef waters. This is likely the result of reef-scale models being unable to capture larger-scale hydrodynamic processes (e.g., those operating on the shelf) that may also contribute significantly to cross-shelf mixing and transport.

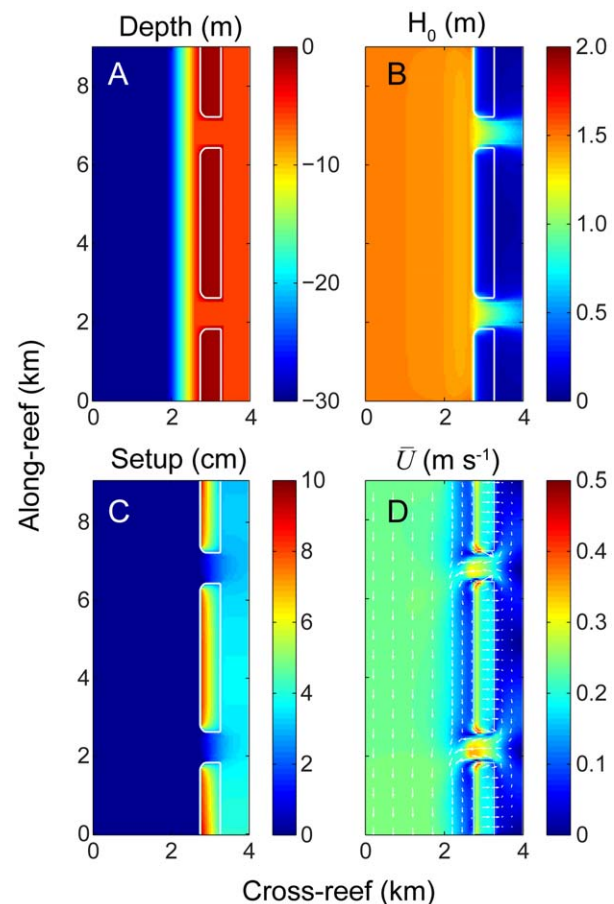


Figure 3. Hydrodynamic simulation results. Variations in A) bathymetry, B) significant wave height, C) setup, and D) depth-averaged flow speed and direction for the central case. doi:10.1371/journal.pone.0053303.g003

Table 5. Hydrodynamic data from all simulations including setup at the reef crest, cross-reef transport and currents observed at the back of the reef flat, and setup in the lagoon, as well as average transport, currents, and average significant wave heights within the channel.

Simulation	η_{crest} cm	q_r $\text{m}^2 \text{s}^{-1}$	\bar{U}_r m s^{-1}	η_{lag} cm	q_c $\text{m}^2 \text{s}^{-1}$	\bar{U}_c m s^{-1}	H_c m
Central Case	8.0	0.21	0.18	3.6	-1.8	-0.30	1.09
$H_0 = 0.5 \text{ m}$	1.2	0.09	0.08	0.6	-0.8	-0.13	0.42
$H_0 = 1 \text{ m}$	4.2	0.15	0.14	1.7	-1.3	-0.21	0.77
$H_0 = 2 \text{ m}$	11.9	0.24	0.22	6.1	-2.2	-0.37	1.38
$H_0 = 3 \text{ m}$	19.5	0.29	0.26	12.8	-2.9	-0.49	1.85
$h_r = 0.5 \text{ m}$	10.3	0.08	0.17	2.5	-1.0	-0.17	1.08
$h_r = 0.7 \text{ m}$	9.2	0.13	0.18	3.1	-1.3	-0.22	1.08
$h_r = 1.5$	6.5	0.27	0.15	4.4	-2.1	-0.36	1.09
$h_r = 2.0 \text{ m}$	5.8	0.28	0.12	4.5	-2.3	-0.38	1.09
$L_r = 250 \text{ m}$	6.7	0.26	0.22	3.9	-2.1	-0.34	1.17
$L_r = 500 \text{ m}$	8.6	0.17	0.15	3.9	-1.6	-0.27	1.00
$L_r = 1000 \text{ m}$	9.1	0.14	0.13	3.8	-1.5	-0.26	0.92
$h_c = 3 \text{ m}$	9.7	0.12	0.11	8.6	-1.1	-0.35	0.85
$h_c = 4.5 \text{ m}$	8.4	0.18	0.16	5.6	-1.5	-0.33	1.01
$h_c = 10 \text{ m}$	7.5	0.24	0.21	1.6	-2.2	-0.22	1.16
$W_c = 200 \text{ m}$	9.2	0.14	0.13	7.6	-3.6	-0.61	0.90
$W_c = 300 \text{ m}$	8.5	0.17	0.15	6.0	-2.9	-0.49	1.00
$W_c = 450 \text{ m}$	8.2	0.19	0.17	4.5	-2.2	-0.37	1.06
$W_c = 1200 \text{ m}$	7.7	0.22	0.20	2.4	-0.9	-0.15	1.11
$\zeta_{\text{sea}} = +0.5 \text{ m}$	5.7	0.30	0.19	4.3	-2.4	-0.37	1.12
$\zeta_{\text{sea}} = +1 \text{ m}$	4.5	0.36	0.17	4.3	-2.8	-0.40	1.15
$\zeta_{\text{sea}} = +2 \text{ m}$	3.4	0.37	0.12	3.4	-3.0	-0.37	1.19
$\zeta_{\text{sea}} = +4 \text{ m}$	1.5	0.23	0.04	1.4	-2.0	-0.20	1.25
$P = 150$	8.0	0.21	0.18	3.6	-1.8	-0.30	1.09
$P = 330$	8.0	0.21	0.18	3.6	-1.8	-0.30	1.09
$P = 1000$	8.0	0.21	0.18	3.6	-1.8	-0.30	1.09
$P = 1500$	8.0	0.21	0.18	3.6	-1.8	-0.30	1.09
$G_{\text{net},P} = 0\%$	8.0	0.21	0.18	3.6	-1.8	-0.30	1.09
$G_{\text{net},P} = 40\%$	8.0	0.21	0.18	3.6	-1.8	-0.30	1.09
$P_{\text{lag}} = 330$	8.0	0.21	0.18	3.6	-1.8	-0.30	1.09
$P_{\text{lag}} = 330, h_c = 3 \text{ m}$	9.7	0.12	0.11	8.6	-1.1	-0.35	0.85
$U_{\text{off}} = 0.125 \text{ m s}^{-1}$	8.0	0.21	0.18	3.6	-1.7	-0.29	1.09
$L_{\text{lag}} = 1500 \text{ m}, h_c = 20 \text{ m}$	7.3	0.25	0.22	0.5	-3.5	-0.17	1.13

All data shown represent values averaged over line transects and zones identified in Fig. 2B.
doi:10.1371/journal.pone.0053303.t005

Since diurnal minima and maxima in carbonate chemistry parameters can be both complex and short-lived for many locations (on real reefs as well as on our model reef), we defined a statistically representative amplitude (A) of diurnal variation in a given carbonate chemistry parameter based on the temporal variance in that parameter value

$$A_{\text{carb}} = \sqrt{2} \sigma_{\text{carb}}(t) \quad (15)$$

where carb represents either TA, DIC, $p\text{CO}_2$, pH, or Ω_{ar} and $\sigma_{\text{carb}}(t)$ is estimated by the standard deviation of the depth-averaged parameter value at a given location from the mean over a 24-hour period. Thus, if the diurnal variation is quasi-sinusoidal,

then the range between minima and maxima will be $\sim 2A_{\text{carb}}$, or roughly $\pm A_{\text{carb}}$ about the mean. We further defined δ_{carb} to represent the ‘net offset’ of TA, DIC, $p\text{CO}_2$, pH, or Ω_{ar} in reef waters relative to offshore waters (Δ_{carb}) averaged over a 24-hour period

$$\delta_{\text{carb}} = \frac{1}{24} \int_0^{24} \Delta_{\text{carb}}(t) dt \quad (16)$$

Defining A_{carb} and δ_{carb} in Eqns. 15 and 16 allowed us to distil the four-dimensional output of our simulations (x, y, z, t) into two-

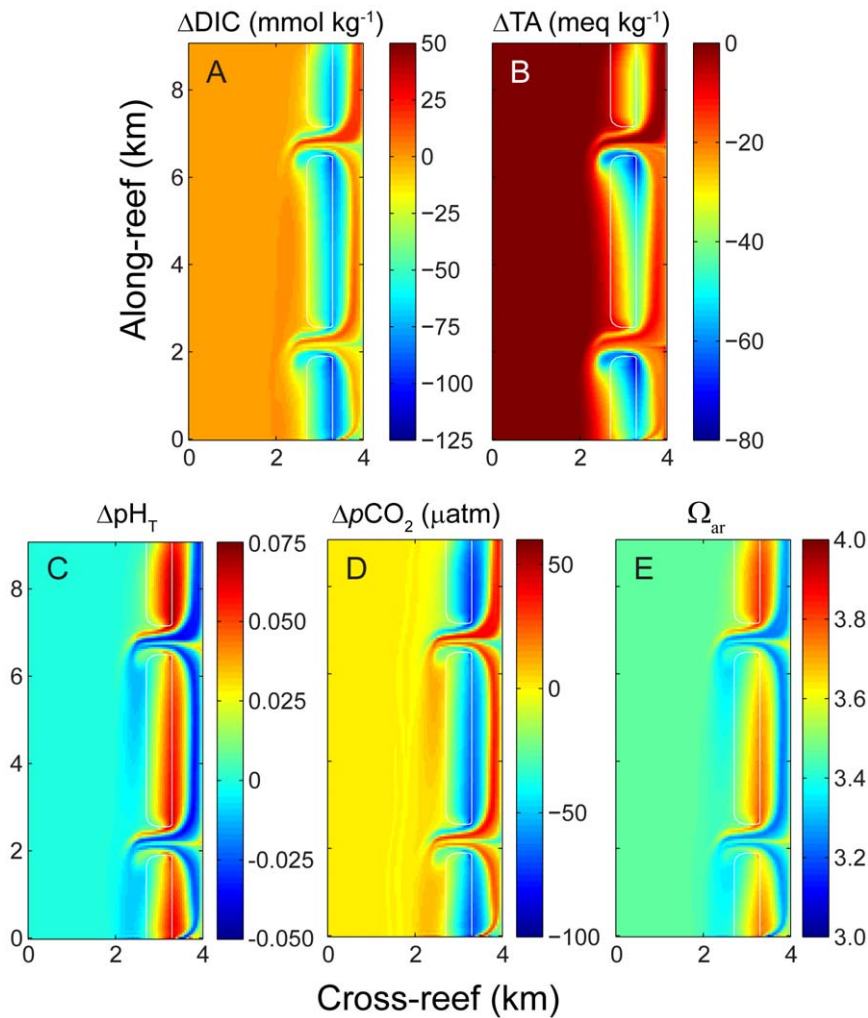


Figure 4. Spatial variation in carbonate chemistry at mid-day. Changes in A) dissolved inorganic carbon, B) total alkalinity, C) pH_T , and D) water column pCO_2 relative to offshore values as well as E) spatial variation in aragonite saturation state at mid-day for the central case. doi:10.1371/journal.pone.0053303.g004

dimensional variables that vary only with location (x, y) through depth- and time-averaging.

Both A_{pCO_2} and δ_{pCO_2} varied across the reef domain, increasing from the shallow forereef to the backreef and lagoon, and reaching maximum levels inside the channels (Fig. 6). Here we define the ‘forereef’ as the reef area seaward of the reef crest but excluding the outer channel, and ‘backreef’ as the point furthest lagoonward but still on the reef flat (see Fig. 2). The full output of A_{carb} and δ_{carb} for TA, DIC, pCO_2 , pH , or Ω_{ar} in each of the three zones and for all 33 simulations are provided in Tables S1 through S5. As waters with altered chemistry exited the channel they became both entrained and diluted by the predominant current as it moved southward. This resulted in noticeable along-reef variations in water chemistry across the reef flat and lagoon. This entrainment effect was particularly pronounced at the boundaries between the reef flats and channels where lagoonward flow across the reef flat and seaward flow out the channels generated notable velocity shear. The re-circulation of waters around eddies generated by these flow features near the channel mouth caused local alterations in water chemistry that were higher than the surrounding reef flat (Fig. 6). Prior numerical studies have shown that these features are less pronounced under more realistically variable hydrodynamic forcing, i.e. as opposed to the stationary

offshore wave forcing assumed in the present study. Therefore, for real reefs we expect these eddies to only influence variations in water chemistry at a local scale (100 s of m) near the edges of channel mouths. Regardless, we would still caution against deriving system-scale budgets from chemical measurements made near these hydrodynamically complex transitions.

Changes in water column pCO_2 varied not only by location, but with the rate of metabolism, degree of wave forcing, and reef geomorphology as well. Sample plots of A_{pCO_2} for select simulations resulting in both weak and strong variation in water column carbonate chemistry are provided as examples in Fig. 7. Higher offshore waves and/or lower rates of benthic metabolism resulted in weaker variations in carbonate chemistry, whereas lower offshore waves and/or higher rates of benthic metabolism resulted in stronger variations in carbonate chemistry. In the interest of distilling this two-dimensional data even further, we next calculated representative A_{pCO_2} and δ_{pCO_2} for key sites within the reef domain by averaging $A_{\text{pCO}_2}(x, y)$ and $\delta_{\text{pCO}_2}(x, y)$ across forereef and backreef transects as well as across most of the lagoon (Fig. 2b). This is because the general pattern of spatial variations in A_{pCO_2} and δ_{pCO_2} across all other simulations were similar to that exhibited by the central model case (Figs. 5, 6); i.e., the spatial

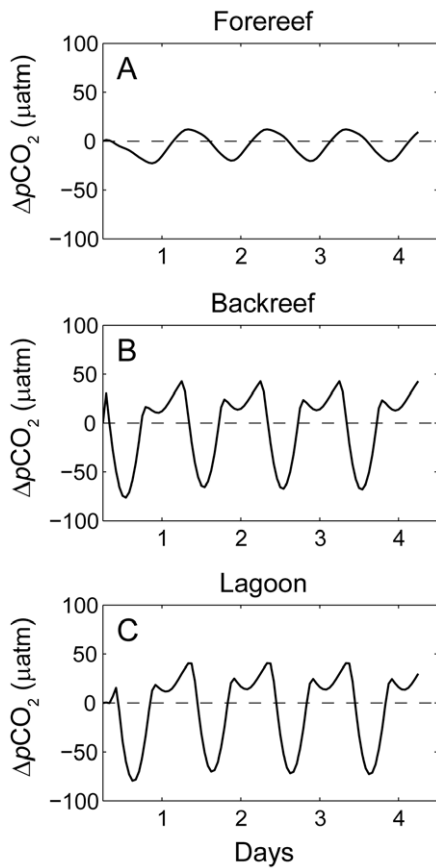


Figure 5. Diurnal variations in water column $p\text{CO}_2$. Changes in dissolved $p\text{CO}_2$ in waters on the A) foreereef, B) backreef, and C) lagoon relative to offshore values for the central case. A four-day simulation was run for the central case and is shown here in its entirety solely to indicate the stability of the model simulation after just one day. For each location shown, the observations were recorded at the centermost point of the foreereef and backreef transects as well as lagoon zone shown in Fig. 2B. The dashed line indicates no change in $p\text{CO}_2$. doi:10.1371/journal.pone.0053303.g005

variation in $A_{p\text{CO}_2}$ and $\delta_{p\text{CO}_2}$ differed mainly in magnitude rather than in structure.

Diurnal changes in $p\text{CO}_2$ across the lagoon were roughly equal in magnitude to and highly correlated with changes on the backreef, whereas diurnal changes in $p\text{CO}_2$ across the foreereef were far more modest in comparison and only weakly correlated with diurnal changes on the backreef (Fig. 8 a,b). This result was not entirely unexpected given the much higher areal rates of benthic metabolism on the reef flat versus in the lagoon (Fig. 3d). However, when we elevated rates of benthic metabolism inside the lagoon (e.g., $P_{\text{lag}} = 330$ vs. $80 \text{ mmol C m}^{-2} \text{ d}^{-1}$) as well as decreased the depth of the lagoon by one-half ($h_c = 3$ vs. 6 m) to simulate the high level of metabolic activity observed in some shallow lagoons [39], $A_{p\text{CO}_2}$ in the lagoon was still just 13% higher than at the backreef (85 vs. $75 \mu\text{atm}$). Although $A_{p\text{CO}_2}$ on the foreereef more than doubled in this simulation relative to the model central case (42 vs. $16 \mu\text{atm}$) due to the mixing and advection of more altered channel outflow waters, the increase in $A_{p\text{CO}_2}$ between the foreereef and backreef was still more than three times greater than the increase in $A_{p\text{CO}_2}$ between the backreef and lagoon (+33 vs. $+10 \mu\text{atm}$). Thus, our results indicate that most of the biologically driven changes in water carbonate chemistry occurred during the relatively short transit across the reef flat

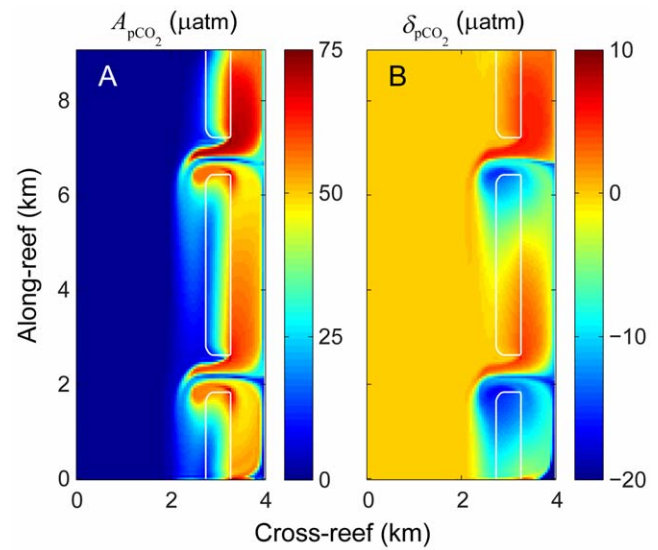


Figure 6. Diurnal and net changes in water column $p\text{CO}_2$. A) Amplitude of diurnal $p\text{CO}_2$ variation ($A_{p\text{CO}_2}$) and B) net offset of $p\text{CO}_2$ relative to offshore waters over a 24-hour period ($\delta_{p\text{CO}_2}$) for the central model case. doi:10.1371/journal.pone.0053303.g006

(20 minutes to 3 hours, median = 50 min); and that lagoon metabolism is a generally far less important source of variation. This preliminary conclusion allows us to focus our remaining analysis primarily on the physical and biogeochemical factors driving variation in $p\text{CO}_2$ across the reef flat itself; specifically those identified in Eq. 7 and Eq. 8.

Predicted functional relationships

To calculate the ratio of metabolic forcing to wave forcing, it is first necessary to establish a representative benthic flux on the reef flat (J_r) with which to calculate J'_r (Eq. 8). For example, changes in DIC are driven by both net production and net calcification (Eq. 14); therefore, diurnal variation in ΔDIC (A_{DIC}) should scale according to the full diurnal range in benthic DIC fluxes. This means that benthic DIC fluxes on the reef flat should vary from a minimum equal to $-r$ to a maximum equal to $np_{\text{max}} + g_{\text{net,max}}$, or a range equal to $p_{\text{max}} + g_{\text{net,max}}$. Given the complex behavior of diurnal species curves (Fig. 5) and given that we are interested in calculating the standard deviation in DIC over the course of the day (Eq. 15), it is more sensible to define a flux scale that is based on the daily integrated rates of benthic metabolism rather than short-lived maximum hourly rates. Furthermore, basing our calculations on daily integrated rates would allow us to make better use of data already reported in the literature (Table 2). Therefore, we defined the following diurnal variation flux for DIC:

$$J_A(\text{DIC}) \equiv P + G_{\text{net}} \quad (17)$$

For the average difference in DIC between reef and offshore waters over a 24-hour period (δ_{DIC}), the relevant flux is the net sum of respiration minus production and net calcification:

$$J_\delta(\text{DIC}) \equiv R - P - G_{\text{net}} \quad (18)$$

such that positive values of $J_\delta(\text{DIC})$ increase DIC, and vice-versa. Following similar logic, we defined the relevant fluxes for both $J_A(\text{TA})$ and $J_\delta(\text{TA})$ to be $2G_{\text{net}}$ and $-2G_{\text{net}}$, respectively. Defining

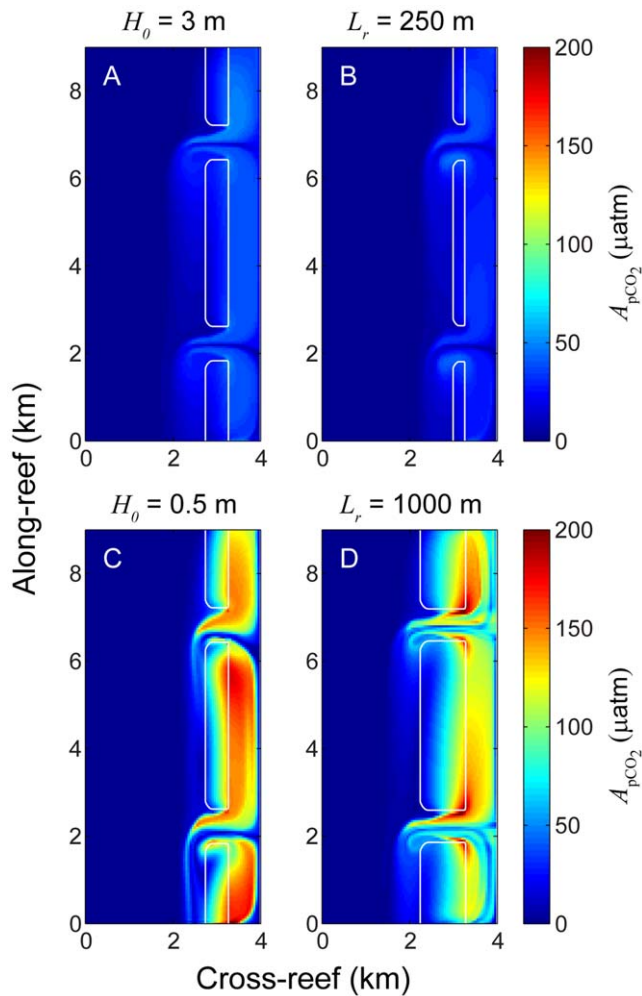


Figure 7. Weak and strong variation in $p\text{CO}_2$. Amplitude of diurnal $p\text{CO}_2$ variation ($A_{p\text{CO}_2}$) for simulations based on the following variations in offshore wave height and reef flat length: A) $H_0 = 3$ m, B) $L_r = 250$ m, C) $H_0 = 0.5$ m, and D) $L_r = 1000$ m. Simulations shown in A and B represent conditions resulting in relatively weak variations in carbonate chemistry while simulations C and D represent conditions resulting in relatively strong variations in carbonate chemistry. doi:10.1371/journal.pone.0053303.g007

equivalent benthic flux scales for dissolved CO_2 requires accounting for the fact that calcification releases less than one mol of CO_2 for each mol of CaCO_3 precipitated [65–67]. Thus, we defined the following benthic fluxes for changes in CO_2

$$J_A(\text{CO}_2) \equiv P - \Psi G_{\text{net}} \quad (19)$$

$$J_\delta(\text{CO}_2) \equiv R - P + \Psi G_{\text{net}} \quad (20)$$

where Ψ is the ratio of moles of CO_2 released per mol of CaCO_3 precipitated and equal to ~ 0.6 for the representative tropical seawater used here ($S = 35$, $T = 25^\circ\text{C}$, average $p\text{CO}_2 = 390$ μatm); however, Ψ can vary between approximately 0.5 and 0.7 in tropical reef systems depending on temperature, salinity, and $p\text{CO}_2$ [66,68]. Finally, because we are keeping temperature and salinity constant within the domain and across all simulations, changes in water column $p\text{CO}_2$ are in constant proportion to

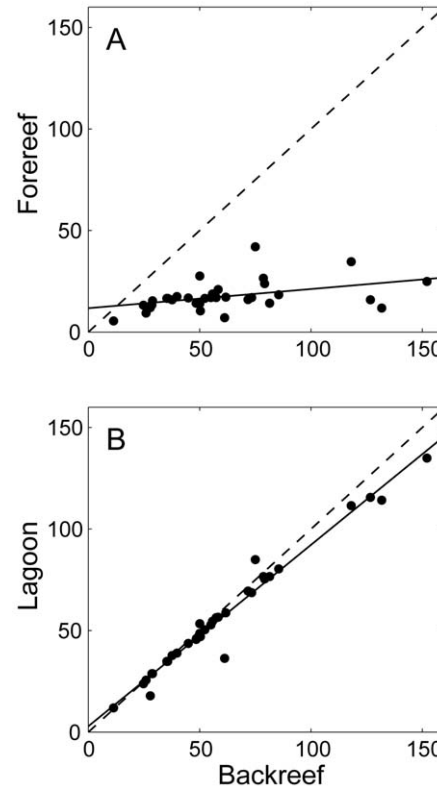


Figure 8. Changes in $p\text{CO}_2$ on the forereef and lagoon versus the backreef. Amplitude of diurnal $p\text{CO}_2$ variation ($A_{p\text{CO}_2}$) A) at the forereef and B) in the lagoon versus the backreef. The solid lines represent best-fit linear regressions in the form of A) $y = 0.09x + 12$, $r^2 = 0.18$ and B) $y = 0.89x + 2.9$, $r^2 = 0.97$ where $n = 33$ for both plots. The dashed lines represent 1:1 relationships. doi:10.1371/journal.pone.0053303.g008

changes in dissolved CO_2 gas concentration ($[\text{CO}_2]_{\text{aq}}$) through a fixed Henry's Law constant (K'_H)

$$p\text{CO}_2 = \frac{[\text{CO}_2]_{\text{aq}}}{K'_H} \quad (21)$$

Thus, for the present study we used Eq. 19 and Eq. 20 to define the benthic fluxes relevant to $A_{p\text{CO}_2}$ and $\delta_{p\text{CO}_2}$, respectively, as well. The individual dependency of A_{carb} and δ_{carb} for TA, DIC, $p\text{CO}_2$, pH, or Ω_{ar} on the ratio of metabolic to wave forcing, reef flat dimensions, and system frictional resistance is provided in Tables S1 through S5.

Changes in water column carbonate chemistry simulated by the three-dimensional model were in close agreement with predictions made by the analytical one-dimensional model. $A_{p\text{CO}_2}$ at the backreef transect increased linearly with J'_r in a manner consistent with that predicted by Eq. 8 (Fig. 9). Thus, $A_{p\text{CO}_2}$ increased with both increasing rates of reef metabolism and decreasing offshore wave heights. Reducing offshore wave heights by a factor of three ($H_0 = 0.5$ vs. 1.5 m) had a roughly equivalent impact on backreef $A_{p\text{CO}_2}$ as tripling rates of benthic production and net calcification (Fig. 9). Backreef $A_{p\text{CO}_2}$ also increased linearly with $L_r^{3/4}$ in a manner consistent with that predicted by Eq. 8 for almost all simulations (Fig. 10). Thus, changes in $p\text{CO}_2$ were highly dependent on the depth and width of the reef flat. However, backreef $A_{p\text{CO}_2}$ in the shallowest reef flat simulation ($h_r = 0.5$) deviated positively from the relationship defined by other

simulations where h_r , L_r or η_{sea} were allowed to vary and all other variables were kept constant. Increasing the offshore sea level (η_{sea}) by just +0.5 m caused a $\sim 30\%$ reduction in A_{pCO_2} at the backreef; however, further increasing sea level from +0.5 to +4 m had little additional effect on backreef A_{pCO_2} . This indicated a limited sensitivity of water column carbonate chemistry to rising sea level or tide if rates of benthic metabolism remain unchanged (Fig. 10). Finally, A_{pCO_2} at the backreef also increased linearly with $\sqrt{f_{sys}}$ in a manner consistent with that predicted by Eq. 8; however, the dependency of A_{pCO_2} on $\sqrt{f_{sys}}$ was far weaker than on J'_r or L_r (Fig. 11).

Increasing the rate of community net calcification relative to gross primary production had only a modest effect on diurnal variations in water column pCO_2 . For example, changing the ratio of $G_{net}:P$ by $\pm 100\%$ (i.e., changing G_{net} from 20% to either 0% or 40% of P) caused A_{pCO_2} at the backreef to change by just $\pm 8\%$ ($52 \pm 4 \mu\text{atm}$), A_{pH} to change by just $\pm 16\%$ (0.047 ± 0.007) and A_{Ω} to change by just $\pm 26\%$ (0.27 ± 0.07). This is because organic carbon metabolism (i.e., production and respiration) is the dominant driver of diurnal variation in water column pCO_2 , pH, and Ω in most coral reef systems. However, net calcification does appear to play an influential role in driving the net offset (δ) of pCO_2 , pH, and Ω over time scales of a day or more. Results from the central case model indicated that the uptake of CO_2 by net production appear to balance the release of CO_2 by net calcification over a 24-hour period such that δ_{pCO_2} at the backreef was just $-1 \mu\text{atm}$. However, increasing the ratio of $G_{net}:P$ to 40% increased the δ_{pCO_2} at the backreef by $+14 \mu\text{atm}$ indicating that net calcification acting as a CO_2 source was over-riding the ability of reef flat net autotrophy to act as a CO_2 sink (Eq. 20). Not surprisingly, decreasing $G_{net}:P$ to 0% had the opposite effect of decreasing δ_{pCO_2} at the backreef by $-15 \mu\text{atm}$. Similarly, increasing the ratio of $G_{net}:P$ to 40% decreased δ_{pH} and $\delta_{\Omega_{ar}}$ at

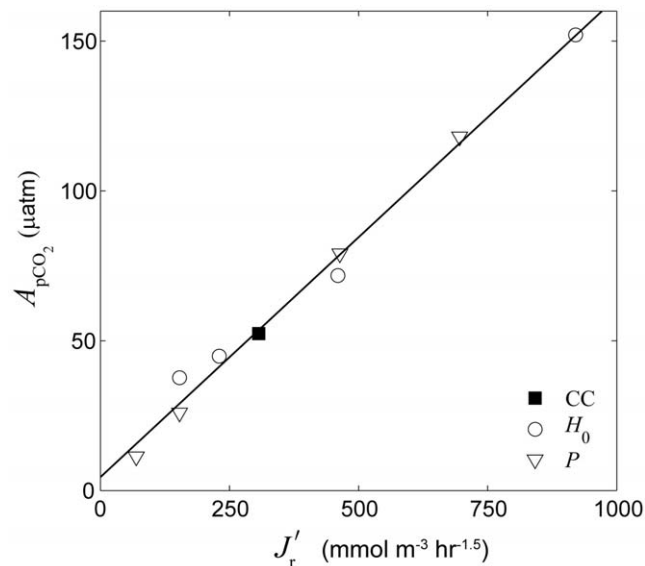


Figure 9. Effect of the ratio of metabolic forcing to wave forcing. Amplitude of diurnal pCO_2 variation (A_{pCO_2}) at the backreef versus J'_r assuming $J_r \equiv P - \Psi G_{net}$ (see Eq. 19). All other variables not listed in the legend were equal to those of the central case ('CC') except for G_{net} which was set equal to 20% of P in all simulations shown. The solid line represents the best-fit linear regression in the form of $y = 0.16x + 4.5$, $r^2 = 0.99$, $n = 9$.
doi:10.1371/journal.pone.0053303.g009

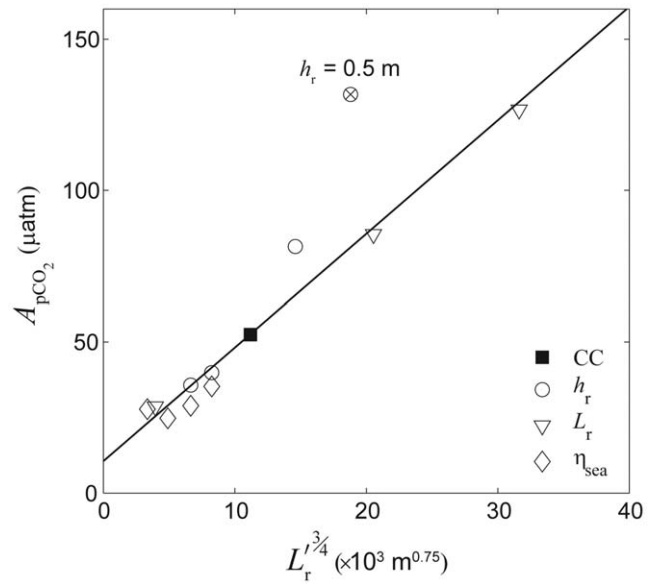


Figure 10. Effect of reef flat geometry. Amplitude of diurnal pCO_2 variation (A_{pCO_2}) at the backreef versus L'_r based on simulations varying reef flat depth, reef flat width, and sea level. All other variables not listed in the legend were equal to those of the central case ('CC'). The solid line represents the best-fit linear regression in the form of $y = 3.8x + 10.6$, $r^2 = 0.96$, $n = 11$. The circle with the cross represents the shallowest reef flat simulation ($h_r = 0.5$ m) and was not included in the regression.
doi:10.1371/journal.pone.0053303.g010

the backreef by 0.02 and 0.17, respectively; whereas decreasing $G_{net}:P$ to 0% increased δ_{pH} and $\delta_{\Omega_{ar}}$ by the similar amounts. Nonetheless, the absolute magnitude of δ_{pCO_2} , δ_{pH} , and $\delta_{\Omega_{ar}}$ in

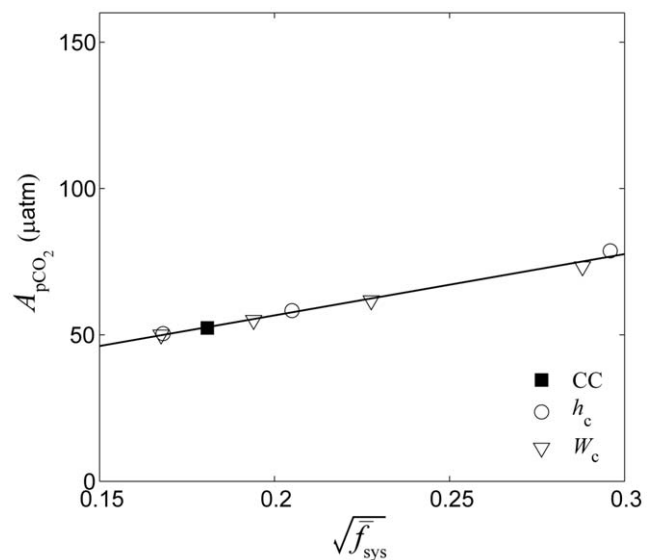


Figure 11. Effect of total system resistance. Amplitude of diurnal pCO_2 variation (A_{pCO_2}) at the backreef versus $\sqrt{f_{sys}}$ based on simulations varying channel depth and width. All other variables not listed in the legend were equal to those of the central case ('CC'). The solid line represents the best-fit linear regression in the form of $y = 210x + 15$, $r^2 = 0.99$, $n = 8$.
doi:10.1371/journal.pone.0053303.g011

backreef waters were always less than 20 μatm , 0.02, and 0.18; respectively, across all simulations.

Discussion

The minor deviation of A_{pCO_2} from a linear dependency on $L_r'^{3/4}$ predicted by Eq. 8 for one very shallow simulation ($h_r = 0.5$ m, see Fig. 10) was largely the result of the frictional resistance of the reef flat increasing dramatically as the depth of the reef flat became less than ~ 1 m (see Fig. 12). This behavior is consistent with prior studies of the response of mean current drag over reef communities to decreasing depth [69–71]. The large increase in the frictional resistance of the reef flat, in turn, caused a substantial increase in the frictional resistance of the reef system as a whole (\bar{f}_{sys}). This further reduced the cross-reef transport which, in turn, increased the contact time of the water with the shallow reef flat leading to greater-than-expected alteration in water chemistry. Otherwise, the dependency of \bar{f}_{sys} on h_r is generally weak when h_r is greater than ~ 0.7 m, such that the influence of h_r on changes in water chemistry is evident mainly through its influence on the reef flat length scale alone (L_r'). Nonetheless, the effect of decreasing h_r on changes in water chemistry will still be captured by Eq. 7, regardless of whether it acts through L_r' or \bar{f}_{sys} .

The particularly weak dependency of A_{pCO_2} on \bar{f}_{sys} was not expected (Fig. 11); however, there are several explanations for this behavior. First, the dependency of ΔC_r on \bar{f}_{sys} given in Eq. 7 is sub-linear ($\Delta C_r \propto \sqrt{\bar{f}_{\text{sys}}}$) meaning that a three-fold increase in \bar{f}_{sys} should a priori cause a less than two-fold increase in ΔC_r . Second, Eq. 3 and Eq. 7 implicitly assume that 1) the gradient in setup driving flow through the channel extends over a distance equal to the length of the reef flat, and 2) that the setup at the entrance of the channel is ~ 0 or equal to the offshore sea level. Our simulations combined with prior studies indicate that cross-reef gradients in setup through the channel are generally weaker and/or more gradual than on the reef flat; extending from beyond the reef crest to well inside the lagoon (Fig. 13a, [40]). This is the result of the inherently two-dimensional structure of both flow and setup adjacent to the channels. Flow converges on the lagoon-side of the channel and then increases seaward as along-reef inflows draining off the adjoining reefs add to the outflow. This acceleration of the channel flow is then partly resisted by setup at the channel entrance due to a gradual decline in landward wave radiation stress (Fig. 3d). Consequently, the actual setup inside the

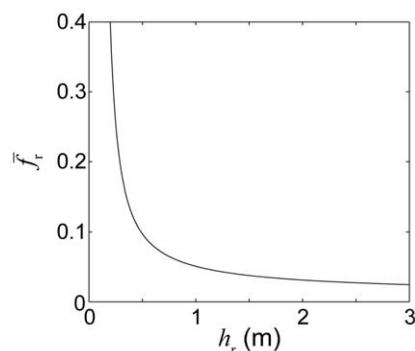


Figure 12. Depth-dependence of bottom friction coefficient. Reef flat bottom friction coefficient versus the average depth of the reef flat.

doi:10.1371/journal.pone.0053303.g012

lagoon has to be greater than that predicted by the one-dimensional analytical model derived in Eq. 3 in order to generate the outflow necessary to balance the corresponding inflow across the reef flat. This means that the ratio of setup (or gravitational potential) in the lagoon to setup at the reef crest is higher than would be predicted by the corresponding ratio of channel to system resistance (Fig. 13b). This non-linear, two-dimensional effect dampens the dynamic response of q_r and ΔC_r to changes in the relative width and depth of the channel further limiting the influence of \bar{f}_{sys} on q_r and ΔC_r . Fortunately, the relationship between $\eta_{\text{lag}}/\eta_{\text{crest}}$ and $\bar{f}_c/\bar{f}_{\text{sys}}$ is still very linear (Fig. 13b) such that the dependency of A_{pCO_2} on $\sqrt{\bar{f}_{\text{sys}}}$ is nonetheless highly linear overall; albeit weaker than expected (Fig. 11).

Taken in total, the combined dependency of A_{pCO_2} on J_r' , L_r' , and \bar{f}_{sys} produced by the three-dimensional model was very consistent with that predicted by the terms shown in Eq. 7 and Eq. 8 derived in our analytical one-dimensional model for all 33 simulations ($r^2 = 0.94$, Fig. 14). Although we developed our numerical model around a flexible idealized reef, average A_{pCO_2} observed in real reef systems showed very good agreement with predictions made by our analytical one-dimensional model as well ($r^2 = 0.94$, Fig. 14). The combined dependency of δ_{pCO_2} on J_r' , L_r' , and \bar{f}_{sys} produced by the three-dimensional model was also very consistent with that predicted by the one-dimensional model assuming the appropriate benthic flux scale for J_δ ($r^2 = 0.76$, Fig. 15). There was also reasonably good agreement between average observed δ_{pCO_2} on real reefs and predictions made by our analytical one-dimensional model ($r^2 = 0.64$, Fig. 15); however, the slope of the regression of observed δ_{pCO_2} versus combined predictive factors was less than that for the idealized simulations (4×10^{-5} vs. 18×10^{-5} $\mu\text{atm m}^{2.25} \text{hr}^{1.5} \text{mmol}^{-1}$, $p < 0.05$). This is largely due to the influence of the data from Bora Bay exhibiting δ_{pCO_2} which clustered around 5 ± 30 μatm despite substantial net

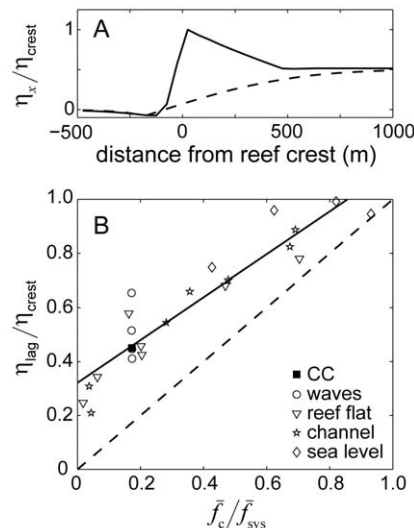


Figure 13. Ratio of wave setup versus ratio of system friction. A) profiles of normalized wave-driven setup across the reef flat (solid line) and channel (dashed line). B) The ratio of lagoon to reef-crest setup versus the ratio of the channel friction coefficient to the total system friction coefficient for simulations testing variation in offshore wave heights, reef flat geometry, channel geometry, and sea level. The solid line represents best-fit regression of the form of $y = 0.8x + 0.32$ ($r^2 = 0.87$, $n = 23$). The dashed line represents a 1:1 relationship.

doi:10.1371/journal.pone.0053303.g013

CO₂ uptake measured in that reef system ($J_{\delta} < 0$). One reason for the larger discrepancy between predicted δ_{pCO_2} versus simulated and observed δ_{pCO_2} in comparison to with A_{pCO_2} is that δ_{pCO_2} was considerably smaller than A_{pCO_2} for both our idealized simulations and for real reefs. In our simulations A_{pCO_2} was ~ 15 times higher than δ_{pCO_2} on average while for the real reef data A_{pCO_2} was ~ 5 times higher than δ_{pCO_2} on average. Such a high signal-to-offset ratio would make the estimates of δ_{pCO_2} from either model simulations or in situ observations far more prone to uncertainty than estimates of A_{pCO_2} . This is likely because the release of CO₂ in most real reefs from calcification and respiration is largely offset by the uptake of CO₂ from photosynthetic production ($J_{CO_2} = \Psi G_{net} + R - P$, [67]) such that most reefs are only modest sources of CO₂ [67,72,73]. The sum of daily integrated CO₂ fluxes for the central model case equaled $(0.6 \times 130) - 660 + 610$ or just $+30 \text{ mmol CO}_2 \text{ m}^{-2} \text{ d}^{-1}$; a value consistent with prior estimates made for coral reefs worldwide ($+10$ to $+30 \text{ mmol CO}_2 \text{ m}^{-2} \text{ d}^{-1}$ [68]). Not only is this CO₂ flux much less than the error in most estimates of either P , R , or G_{net} alone [24,26,45], it ultimately produced δ_{pCO_2} of just -1 to $-2 \text{ } \mu\text{atm}$ in backreef and lagoon waters given typical offshore wave heights, reef dimensions, and rates of benthic metabolism.

Tides can provide another source of variation in δ_{pCO_2} for real reefs that were not explicitly considered in the present simulations. Most tidal modes occur on periods that are not perfectly in phase with the 24-hour diurnal cycle causing the minimum and maximum tidal elevations to occur at different times of day. This,

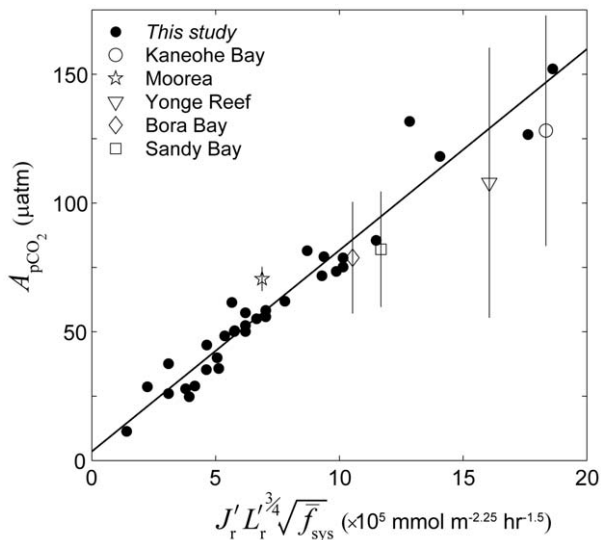


Figure 14. Combined effect of all factors on diurnal pCO_2 variations. Amplitude of diurnal pCO_2 variation (A_{pCO_2}) of back reef waters versus the combined influence of wave forcing, sea level, metabolism, reef flat geometry, and system frictional resistance for all 33 simulations (dark circles, see Eq. 7 and Eq. 8). For all data shown, J_r' was calculated assuming $J_A \equiv P - \Psi G_{net}$ (see Eq. 19). The solid line represents a best-fit linear regression of the simulations in the form of $y = 7.8x + 3.5$ (MSE = 8 μatm , $r^2 = 0.94$, $n = 33$). Also shown are the average diurnal pCO_2 variation amplitudes observed in real reef systems [24,25,56,57] normalized to a temperature of 25°C (see Eq. 21) for which there was enough supporting hydrodynamic and biogeochemical data (see Tables 2 and 3; the vertical lines represent ± 1 std. dev.). The best-fit regression for the observed mean A_{pCO_2} versus the x-axis term is $y = 5x + 29$ (MSE = 7 μatm , $r^2 = 0.94$, $p < 0.005$, $n = 5$, not shown) and is not significantly different from the regression derived from the model simulations ($p > 0.25$). doi:10.1371/journal.pone.0053303.g014

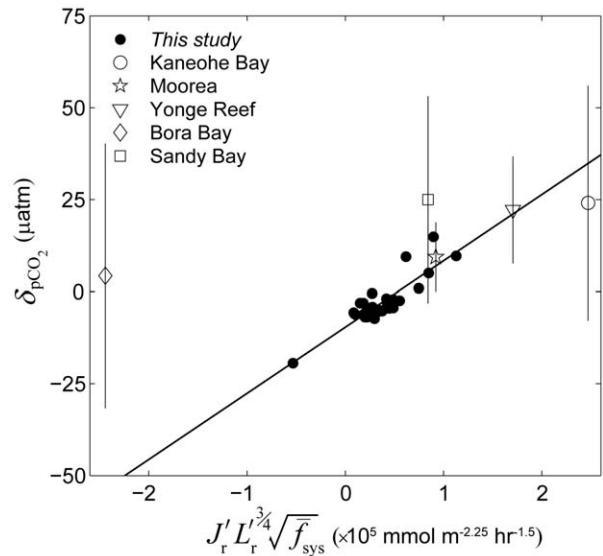


Figure 15. Combined effect of all factors on the net offset in pCO_2 . Difference between the pCO_2 of backreef waters and offshore waters averaged over a 24-hour period (δ_{pCO_2}) versus the combined influence of wave forcing, sea level, metabolism, reef flat geometry, and system frictional resistance for all 33 simulations (dark circles, see Eq. 7 and Eq. 8). For all data shown, J_r' was calculated assuming $J_{\delta} \equiv \Psi G_{net} - P + R$ (see Eq. 20). The solid line represents a best-fit linear regression of the simulations in the form of $y = 18x - 9.6$ (MSE = 3 μatm , $r^2 = 0.76$, $n = 33$). Also shown are the average offsets in the pCO_2 of reef waters relative to offshore waters observed in real reef systems [24,25,56,57] normalized to a temperature of 25°C (see Eq. 21) for which there was enough supporting hydrodynamic and biogeochemical data (see Tables 2 and 3; the vertical lines represent ± 1 std. dev.). The best-fit regression for the observed δ_{pCO_2} versus the x-axis term is $y = 4x + 14$ (MSE = 7 μatm , $r^2 = 0.64$, $p < 0.06$, $n = 5$, not shown). doi:10.1371/journal.pone.0053303.g015

in turn, causes continually varying phase differences between the lows and highs of a strongly diurnal tide and the maximum and minimum rates of benthic metabolism [33]. Consequently, δ_{pCO_2} will be much more negative on days when low tides occur at mid-day and much more positive on days when low tides occur at night (a similar logic can be applied to the other carbonate species). Where tidal variations are large (> 2 m), such phase-driven deviations in carbonate chemistry can be quite large [30]; especially given the synergistic effects of very shallow reef flats on amplifying the metabolic signal as well as decreasing cross-reef transport through increased frictional resistance (Fig. 10). We did not pursue such tidal-interaction simulations given the computational expense of running all of the simulations over a full lunar cycle (~ 1 month) and given prior results showing that differences in tidal phase affected changes in carbonate chemistry mainly through their influence on overall mean sea level [33] (the latter being captured in our simulations). Regardless, these phase-driven positive and negative deviations in δ_{pCO_2} should offset one another when averaged over several weeks or more resulting in long-term δ_{pCO_2} that approach values similar to those we report here. The present model may not apply, however, to extreme low tide conditions when offshore sea level plus wave-driven setup is below the level of the reef crest and wave-driven flow may cease to occur.

Our results indicate that many wave-driven reef systems will be unable to sustain dramatic net long-term changes in their carbonate chemistry relative to offshore waters given typical rates of benthic metabolism, reef morphology, wave forcing, and

frictional resistance. There are examples of reef systems with seasonally higher backreef or lagoon δ_{pCO_2} ($>50 \mu\text{atm}$ [23,25,30]), but these higher values are probably as dependent on the physical characteristics of the specific reef system (e.g., wave forcing, morphology, and sea level) as they are on the summary effects of production, respiration, and calcification on net CO_2 fluxes. Furthermore, in the present study we defined δ_{pCO_2} relative to offshore waters that were in equilibrium with the atmosphere. It is not uncommon, however, for the carbonate chemistry of offshore waters to be in disequilibrium with the atmosphere due to oceanic processes such as upwelling, net pelagic production, and those affecting the gas solubility of surface waters [23,24,74,75]. Such larger-scale ocean processes may explain why long-term differences between the pCO_2 of reef waters and that of the atmosphere are often much greater than long-term differences between the pCO_2 of reef waters and offshore waters (i.e., δ_{pCO_2}), especially on seasonal time scales [23]. This is well beyond the scope of the present study, but should be considered in future investigations.

Larger reef systems and atolls

Our simulations focused mainly on coastally bound reef-lagoon systems with modest lagoon sizes ($L_{lag} \leq 1500 \text{ m}$) and residence times that ranged from several hours to just over a day. This raises the question of whether variations in lagoon carbonate chemistry differ for much larger reef systems with lagoons that are tens of kilometers in size (e.g., New Caledonia; Kwajalein and Majuro in the Marshall Islands; Chuuk and Ulithi in Micronesia; Rangiroa, Tikehau, Muraroa and Ahe in French Polynesia; Huvadho and Ari in the Maldives; Glovers Reef and Lighthouse Reef in Belize; Bermuda in the west Atlantic; etc.) and whose residence times vary from weeks to months [76–79]. Our results, however, indicated that most of the changes in carbonate chemistry occurred over the reef flat and that changes in carbonate chemistry within the lagoon decreased with increasing lagoon volume (Fig. 16). Interestingly, the size of reef flats tend to remain relatively constrained (generally 200 to 1000 m, [80]) even though the size of reef lagoons range by roughly two orders of magnitude (e.g., compare $\sim 50 \text{ km}$ for Chuuk, Micronesia versus 0.5 km for Sandy Bay, Ningaloo Reef, Australia). Given the well-defined range of benthic reef flat metabolic rates as well (Table 2), this implies that the submerged reef rims of large atolls should be of roughly the same size and reactivity as those found on nearshore fringing reef-lagoon systems. Furthermore, previous work has shown that the $P:R$ ratio for entire reef systems are even closer to unity than for individual reef zones; thus, indicating that net CO_2 fluxes decrease when integrating over increasingly larger spatial scales [39]. In fact, both prior and ongoing observations have shown that net offsets in the pCO_2 of lagoon waters relative to offshore were less than $30 \mu\text{atm}$ on average inside Majuro atoll ($10 \text{ km} \times 40 \text{ km}$, $h_{lag} = 35 \text{ m}$, [81]), less than $30 \mu\text{atm}$ inside the Great Barrier Reef ($\sim 50 \text{ km} \times \sim 2,000 \text{ km}$, $h_{lag} = 35 \text{ m}$, [82]), and generally less than $50 \mu\text{atm}$ inside Chuuk atoll ($50 \text{ km} \times 50 \text{ km}$, $h_{lag} = 50 \text{ m}$, <http://www.pmel.noaa.gov/co2>). These changes are modest in comparison with the hundreds of μatm increase in pCO_2 anticipated to occur over the 21st century.

Given that net ecosystem production becomes smaller with increasing spatial and temporal scales, long-term changes in the carbonate chemistry of deep lagoons should be driven more by the release of TA from the dissolution of lagoon sediments:

$$\Delta TA_{lag} = \frac{2d_{sed}\tau_{lag}}{h_{lag}} \quad (22)$$

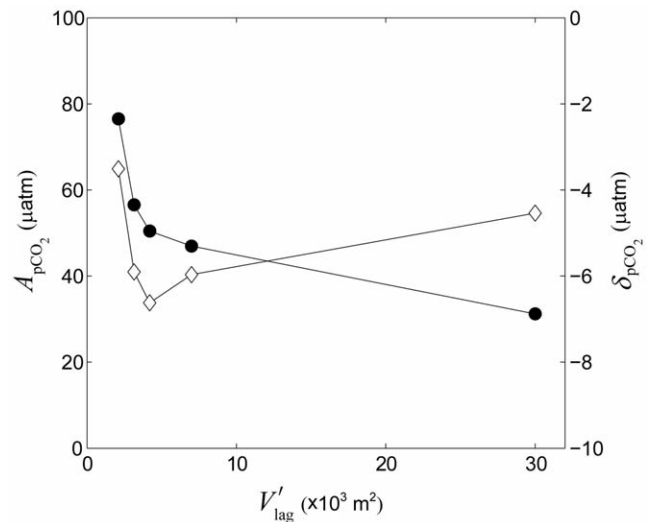


Figure 16. Changes in pCO_2 versus lagoon volume. Amplitude of diurnal pCO_2 variation (closed circles, left y-axis) and net offset in the pCO_2 of lagoon waters relative to offshore waters over a 24-hour period (open diamonds, right y-axis) versus lagoon volume per width of reef flat ($V'_{lag} = h_{lag} \times L_{lag}$). doi:10.1371/journal.pone.0053303.g016

where d_{sed} is the rate of sediment carbonate mineral dissolution and τ_{lag} is the residence time of lagoon waters with respect to surrounding ocean. Rates of dissolution in carbonate sediments of reef systems range between 0.0004 to $0.8 \text{ mmol m}^{-2} \text{ hr}^{-1}$ with a median value of $\sim 0.3 \text{ mmol m}^{-2} \text{ hr}^{-1}$ or $\sim 7 \text{ mmol m}^{-2} \text{ d}^{-1}$ [83]. Assuming a τ_{lag} of 1 to 2 months [77–79] and an average lagoon depth of 46 m [84] for larger atolls, then these lagoons should exhibit long-term increases in TA relative to waters flowing off the reef flat on the order of just $\sim 10 \mu\text{eq kg}^{-1}$. This suggests that variations in carbonate chemistry within such deep lagoons could be more influenced by planktonic growth and metabolism [85]. We caution that reef systems enclosing large but shallow lagoons with long residence times ($>$ weeks) and/or populated by a high density of shallow patch reefs (e.g., Bermuda or Glovers Reef, Belize) could exhibit even greater longer-term shifts in carbonate chemistry relative to offshore waters. Regardless, any additional long-term offsets in lagoon water column carbonate chemistry could be roughly estimated by applying the appropriate variation of Eq. 22 using spatially averaged rates of benthic net production or net calcification [86,87], and adding them to net changes in the carbonate chemistry of waters exported from the reef flat as predicted by the present model (δ_r).

Conclusions

The main objective of the present study was to demonstrate and to better understand how spatial and temporal variation in water column carbonate chemistry are influenced by the different physical and biogeochemical attributes of a reef system acting in combination, not just by rates of benthic metabolism alone. Our results combined with data in the literature allow us to conclude the following: Firstly, most of the changes in carbonate chemistry occur during the transit of water across the reef flat, although these changes can be further augmented by particularly high rates of metabolism in shallow lagoons. Secondly, changes in carbonate chemistry are as sensitive to the combined length and depth of the reef flat as they are on the ratio of metabolic to wave forcing; however, they are much less sensitive to variations in channel

morphology and to the overall frictional resistance of the reef system. Thirdly, the long-term (weeks to months) net offset in water column $p\text{CO}_2$ relative to offshore waters for many reef systems is likely to be marginal due to 1) the release of CO_2 from net community calcification being mostly offset by the uptake of CO_2 from net community production, and 2) physically constrained limits on wave-driven circulation, the length and depth of the reef flat, and the overall frictional resistance of the entire reef system. More importantly, our results demonstrate that it is not possible to properly interpret observed spatial and temporal variations in water column carbonate chemistry, nor to determine the significance of these observations with respect to reef systems in general, without adequate hydrodynamic and morphological data. We suggest that future field studies and monitoring programs aimed at tracking the in situ impacts of ocean acidification on coral reef systems collect such physical information in addition to detailed measurements of water column chemistry. The analytical model we present here thus provides an additional tool to advance these efforts in wave-driven coral reef systems worldwide.

Supporting Information

Appendix S1 Derivation of wave setup formulation.

(DOC)

Appendix S2 Derivation of cross-reef transport formulation.

(DOC)

Appendix S3 Bottom current drag formulations.

(DOC)

Appendix S4 Net production and net calcification parameterizations.

(DOC)

Movie S1 Time-dependent changes in the depth-averaged Total Alkalinity (TA) of reef waters relative to offshore waters over a 24-hour period.

(WMV)

Movie S2 Time-dependent changes in the depth-averaged Dissolved Inorganic Carbon (DIC) of reef waters relative to offshore waters over a 24-hour period.

(WMV)

Movie S3 Time-dependent changes in the depth-averaged $p\text{CO}_2$ of reef waters relative to offshore waters over a 24-hour period.

(WMV)

Movie S4 Time-dependent changes in the depth-averaged pH of reef waters relative to offshore waters over a 24-hour period.

(WMV)

Movie S5 Time-dependent changes in the depth-averaged aragonite saturation state of reef waters relative to offshore waters over a 24-hour period.

(WMV)

Table S1 Variation amplitude and time-average difference in depth-averaged Total Alkalinity (TA) between reef waters and offshore waters over a 24-hour period.

(DOC)

Table S2 Variation amplitude and time-average difference in depth-averaged Dissolved Inorganic Carbon (DIC) between reef waters and offshore waters over a 24-hour period.

(DOC)

Table S3 Variation amplitude and time-average difference in depth-averaged $p\text{CO}_2$ between reef waters and offshore waters over a 24-hour period.

(DOC)

Table S4 Variation amplitude and time-average difference in depth-averaged pH between reef waters and offshore waters over a 24-hour period.

(DOC)

Table S5 Variation amplitude and time-average difference in depth-averaged aragonite saturation state between reef waters and offshore waters over a 24-hour period.

(DOC)

Acknowledgments

This paper benefitted from the helpful comments of two anonymous reviewers.

Author Contributions

Conceived and designed the experiments: JLF RJL. Performed the experiments: JLF ZZ. Analyzed the data: JLF. Contributed reagents/materials/analysis tools: JLF RJL ZZ. Wrote the paper: JLF RJL ZZ MM.

References

- Caldeira K, Wickett ME (2003) Anthropogenic carbon and ocean pH. *Nature* 425: 365.
- Doney SC, Fabry VJ, Feely RA, Kleypas JA (2009) Ocean acidification: the other CO_2 problem. *Ann Rev Marine Sci* 1: 169–192.
- Feely RA, Sabine CL, Lee K, Berelson W, Kleypas J, et al. (2004) Impact of anthropogenic CO_2 on the CaCO_3 system in the oceans. *Science* 305: 362–366.
- Hoegh-Guldberg O, Mumby PJ, Hooten AJ, Steneck RS, Greenfield P, et al. (2007) Coral reefs under rapid climate and ocean acidification. *Science* 318.
- Kleypas JA, Buddemeier RW, Archer D, Gattuso J-P, Langdon C, et al. (1999) Geochemical consequences of increased atmospheric carbon dioxide on coral reefs. *Science* 284: 118–120.
- Silverman J, Lazar B, Cao L, Caldeira K, Erez J (2009) Coral reefs may start dissolving when atmospheric CO_2 doubles. *J Geophys Res* 36.
- Atkinson MJ, Cuet P (2008) Possible effects of ocean acidification on coral reef biogeochemistry: topics for research. *Mar Ecol Prog Ser* 373: 249–256.
- Kleypas J, Langdon C (2006) Coral reefs and changing seawater chemistry. In: Phinney JT, Hoegh-Guldberg O, Kleypas J, Skirving W, Strong A, editors. *Coral Reefs and Climate Change: Science and Management*. Washington, D.C.: Am. Geophys. Union. pp. 73–110.
- Marubini F, Ferrier-Pages C, Furla P, Allemand D (2008) Coral calcification responds to seawater acidification: a working hypothesis towards a physiological mechanism. *Coral Reefs* 27: 491–499.
- Tambutte S, Holcomb M, Ferrier-Pages C, Reynaud S, Tambutte E, et al. (2011) Coral biomineralization: From the gene to the environment. *J Exp Mar Biol Ecol* 408: 58–78.
- Chan NCS, Connolly SR (2012) Sensitivity of coral calcification to ocean acidification: a meta-analysis. *Global Change Biol*: 1–9.
- McCulloch M, Falter JL, Trotter J, Montagna P (2012) Resilience of coral calcification to ocean acidification and global warming: the role of pH up-regulation. *Nature Climate Change*.
- Kurihara H (2008) Effects of ocean acidification on marine ecosystems. *Mar Ecol Prog Ser* 373: 275–284.
- Munday PL, Dixon DL, McCormick MI, Meekan M, Ferrari MCO, et al. (2010) Replenishment of fish populations is threatened by ocean acidification. *Proc Nat Acad Sci* 107: 12930–12934.
- Munday PL, Leis JM, Lough JM, Paris CB, Kingsford MJ, et al. (2009) Ocean acidification impairs olfactory discrimination and homing ability of a marine fish. *Proc Nat Acad Sci* 106: 1848–1852.

16. Kamiewska P, Campbell PR, Kline DI, Rodriguez-Lanetty M, Miller DJ, et al. (2012) Major cellular and physiological impacts of ocean acidification on a reef building coral. *PLoS ONE* 7: e34659.
17. Kohn AJ, Helfrich P (1957) Primary organic productivity of a Hawaiian coral reef. *Limnol Oceanogr* 2: 241–251.
18. Odum HT, Odum EP (1955) Trophic structure and productivity of a windward coral reef community on Eniwetok Atoll. *Ecol Monogr* 25: 1415–1444.
19. Sargent MA, Austin TS (1949) Organic productivity of an atoll. *Trans Amer Geophys Union* 30: 245–249.
20. Smith SV (1973) Carbon dioxide dynamics: A record of organic carbon production, respiration, and calcification in the Eniwetok reef flat community. *Limnol Oceanogr* 18: 106–120.
21. Meinshausen M, Meinshausen N, Hare W, Raper SCB, Frieler K, et al. (2009) Greenhouse-gas emission targets for limiting global warming to 2°C. *Nature* 458: 1158–1162.
22. Friederich T, Timmerman A, Abe-Ouchi A, Bates NR, Chikamoto MO, et al. (2012) Detecting regional anthropogenic trends in ocean acidification against natural variability. *Nature Climate Change* 2: 167–171.
23. Bates NR, Amat A, Andersson AJ (2010) Feedbacks and responses of coral calcification on the Bermuda reef system to seasonal changes in biological processes and ocean acidification. *Biogeosciences* 7: 2509–2530.
24. Falter JL, Lowe RJ, Atkinson MJ, Cuet P (2012) Seasonal coupling and decoupling of calcification rates from coral reef metabolism and carbonate chemistry at Ningaloo Reef, Western Australia. *J Geophys Res Oceans* 117: 14 pp.
25. Shamberger KEF, Feely RA, Sabine CL, Atkinson MJ, DeCarlo EH, et al. (2011) Calcification and organic production on a Hawaiian coral reef. *Mar Chem* 127: 64–75.
26. Silverman J, Lazar B, Erez J (2007) Community metabolism of a coral reef exposed to naturally varying dissolved inorganic nutrient loads. *Biogeochemistry* 84: 67–82.
27. Anthony KRN, Kleypas J, Gattuso JP (2011) Coral reefs modify their seawater carbon chemistry - implications for impacts of ocean acidification. *Global Change Biol* 17: 3655–3666.
28. Broecker WS, Langdon C, Takahashi T, Peng T-S (2001) Factors controlling the rate of CaCO₃ precipitation on the Grand Bahama Bank. *Global Biogeochem Cycles* 15: 589–596.
29. Kleypas J, Anthony KRN, Gattuso JP (2011) Coral reefs modify their seawater carbon chemistry - Case study from a barrier reef (Moorea, French Polynesia). *Global Change Biol* 17: 3667–3678.
30. Shaw EC, McNeil BI, Tilbrook B (2012) Impacts of ocean acidification in naturally variable coral reef flat ecosystems. *J Geophys Res -Oceans* 117: 14 pp.
31. Broecker WS, Peng T-H (1982) *Tracers in the sea*: Eldigio Press, Lamont-Doherty Geological Observatory. 690 p.
32. Jouan A, Douillet P, Oiuillon S, Fraunie P (2006) Calculations of hydrodynamic time parameters in a semi-opened coastal zone using a 3D hydrodynamic model. *Cont Shelf Res* 26: 1395–1415.
33. Zhang Z, Falter JL, Lowe R, Ivey G (2012) The combined influence of hydrodynamic forcing and calcification on the spatial distribution of alkalinity in a coral reef system. *J Geophys Res* 117: 18 pp.
34. Lowe RJ, Falter JL, Monismith SG, Atkinson MJ (2009) Numerical model of wave transformation and circulation within a barrier reef-lagoon system: Kaneohe Bay, Hawaii. *J Geophys Res* 114.
35. Taebi S, Lowe RJ, Pattiaratchi CB, Ivey G, Symonds G, et al. (2011) Nearshore circulation in a tropical fringing reef system. *J Geophys Res* 116.
36. Hoeke R, Storlazzi C, Ridd PV (2011) Hydrodynamics of a bathymetrically complex fringing coral reef embayment: Wave climate, in situ observations, and wave prediction. *J Geophys Res -Oceans* 116: 19.
37. Zhang Z, Lowe RJ, Falter JL, Ivey G (2011) A numerical model of wave- and current-driven nutrient uptake by coral reef communities. *Ecol Modelling* 222: 1456–1470.
38. Lowe RJ, Hart C, Pattiaratchi CB (2010) Morphological constraints to wave-driven circulation in coastal reef-lagoon systems: A numerical study. *J Geophys Res -Oceans* 115: 13 pp.
39. Kinsey DW (1985) Metabolism, calcification, and carbon production: I. Systems level studies. Tahiti. pp. 505–526.
40. Lowe RJ, Falter JL, Monismith SG, Atkinson MJ (2009) Wave-driven circulation of a coastal reef-lagoon system. *J Phys Oceanogr*: DOI: 10.1175/2008JPO3958.1171.
41. Gourlay MR, Colleter G (2005) Wave-generated flow on coral reefs—an analysis for two-dimensional horizontal reef-tops with steep faces. *Coastal Eng* 52: 353–387.
42. Dean RG, Dalrymple RA (1991) *Water wave mechanics for engineers and scientists*; Liu PL-F, editor. Singapore: World Scientific Publishing. 353 p.
43. Hench JL, Leichter JJ, Monismith SG (2008) Episodic circulation and exchange in a wave-driven coral reef and lagoon system. *Limnol Oceanogr* 53: 2681–2694.
44. Falter JL, Atkinson MJ, Schar DW, Lowe RJ, Monismith SJ (2011) Short-term coherency between gross primary production and community respiration in an algal-dominated reef flat. *Coral Reefs* 30: 53–58.
45. Falter JL, Lowe RJ, Atkinson MJ, Monismith SG, Schar DW (2008) Continuous measurements of net production over a shallow reef community using a modified Eulerian approach. *J Geophys Res* 113: 1–14.
46. Mass T, Einbinder S, Brokovich E, Shashar N, Vago R, et al. (2007) Photoacclimation of *Stylophora pistillata* to light extremes: metabolism and calcification. *Mar Ecol Prog Ser* 334: 93–102.
47. Shchepetkin AF, McWilliams JC (2005) The Regional Ocean Modelling System: A split-explicit, free-surface, topography following coordinates ocean model. *Ocean Modelling* 9: 347–404.
48. Booij N, Ris RC, Holthuijsen LH (1999) A third-generation wave model for coastal regions, 1, Model description and validation (Paper 98JC02622). *J Geophys Res* 104(C4): 7649.
49. Warner JC, Sherwood CR, Signell RP, Harris CK, Arango HG (2008) Development of a three-dimensional, regional, coupled wave, current and sediment-transport model. *Computers & Geosci* 34: 1284–1306.
50. Hearn CJ (1999) Wave-breaking hydrodynamics within coral reef systems and the effect of changing sea level. *J Geophys Res* 104: 30,007–30,019.
51. Kraines SB, Yanagi T, Isobe M, Komiyama H (1998) Wind-wave driven circulation on the coral reef at Bora Bay, Miyako Island. *Coral Reefs* 17: 133–143.
52. Soulsby RL (1995) Bed shear-stresses due to combined waves and currents. In: Stive MJF, de Vriend HJ, Fredsoe J, Hamm L, Soulsby RL, et al., editors. *Advances in Coastal Morphodynamics*. Delft, Netherlands: Delft Hydraulics. pp. 20–23.
53. Clavier J, Garrigue C (1999) Annual sediment primary production and respiration in a large coral reef lagoon (SW New Caledonia). *Mar Ecol Prog Ser* 191: 79–89.
54. Glud RN, Eyre BD, Patten NL (2008) Biogeochemical responses to mass coral spawning at the Great Barrier Reef: Effects on respiration and primary production. *Limnol Oceanogr* 53: 1014–1024.
55. Uthicke S, Klumpp DW (1998) Microphytobenthos community production at a near-shore coral reef: seasonal variation and response to ammonium recycled by holothurians. *Mar Ecol Prog Ser* 169: 1–11.
56. Kraines S, Suzuki Y, Omori T, Shitashima K, Kanahara S, et al. (1997) Carbonate dynamics of the coral reef system at Bora Bay, Miyako Island. *Mar Ecol Prog Ser* 156: 1–16.
57. Frankignoulle M, Gattuso JP, Biondo R, Bourge I, Copin-Montegut G, et al. (1996) Carbon fluxes in coral reefs. II. Eulerian study of inorganic carbon dynamics and measurement of air-sea CO₂ exchanges. *Mar Ecol Prog Ser* 145: 123–132.
58. Lee K, Tong LT, Millero FJ, Sabine CL, Dickson AG, et al. (2006) Global relationships of total alkalinity with salinity and temperature in surface waters of the world's oceans. *Geophys Res Letters* 33: 5 pp.
59. Lewis EW, Wallace DWR (1998) Program Developed for CO₂ System Calculations. In: Center CDIA, editor: Oak Ridge National Laboratory, U.S. Department of Energy.
60. Dickson AG, Millero FJ (1987) A comparison of the equilibrium constants for the dissociation of carbonic acid in seawater media. *Deep-Sea Res* 34: 1733–1743.
61. Dickson AG (1990) Standard potential of the reaction: AgCl(s)+1/2H₂(g)=Ag(s)+HCl(aq) and the standard acidity constant of the ion HSO₄⁻ in synthetic seawater from 273/15 to 318.15K. *J Chem Thermodyn* 22: 113–127.
62. Dickson AG (1990) Thermodynamics of the dissociation of boric acid in synthetic seawater from 273.15 to 318.15K. *Deep-Sea Res* 40: 107–118.
63. Mucci CN, Riley JP (1971) The solubility of calcite and aragonite in seawater at various salinities, temperatures, and one atmospheric total pressure. *Amer J Sci* 283: 781–799.
64. Hearn CJ, Parker IN (1988) Hydrodynamic processes on the Ningaloo coral reef, Western Australia. Australia. pp. 497–502.
65. Broecker WS, Takahashi T (1966) Calcium carbonate precipitation of the Bahama Banks. *J Geophys Res* 71: 1575–1602.
66. Frankignoulle M, Canon C, Gattuso J-P (1994) Marine calcification as a source of carbon dioxide: Positive feedback of increasing atmospheric CO₂. *Limnol Oceanogr* 39: 458–462.
67. Gattuso JP, Frankignoulle M, Smith SV (1999) Measurement of community metabolism and significance in the coral reef CO₂ source-sink debate. *Proc Nat Acad Sci* 96: 13017–13022.
68. Ware JR, Smith SV, Reaka-Kudla ML (1991) Coral reefs: sources or sinks of atmospheric CO₂. *Coral Reefs* 11: 127–130.
69. McDonald CB, Koseff JR, Monismith SG (2006) Effects of the depth to coral height ratio on drag coefficients for unidirectional flow over coral. *Limnol Oceanogr* 51: 1294–1301.
70. Rosman JH, Hench JL (2011) A framework for understanding drag parameterizations for coral reefs. *J Geophys Res* 116: 15 pp.
71. Lowe RJ, Shavit U, Falter JL, Koseff JR, Monismith SG (2008) Modeling flow in coral communities with and without waves: a synthesis of porous media and canopy flow approaches. *Limnol Oceanogr* 53: 2668–2680.
72. Smith SV (1995) Reflections on the measurement and significance of carbon metabolism on coral reefs. *Kansas Geological Survey*. 1–18 p.
73. Smith SV, Vech HH (1989) Mass balance of biogeochemically active materials (C,N,P) in a hypersaline gulf. *Est Coast Shelf Sci* 29.
74. Gledhill DK, Wanninkhof R, Millero FJ, Eakin CM (2008) Ocean acidification of the Greater Caribbean Region 1996–2006. *J Geophys Res* 113.
75. Manzello DP (2010) Ocean acidification hot spots: Spatiotemporal dynamics of the seawater CO₂ system of eastern Pacific coral reefs. *Limnol Oceanogr* 55: 239–248.

76. Andrefouet S, Pages J, Tartanville B (2001) Water renewal time for classification of atoll lagoons in the Tuamotu Archipelago (French Polynesia). *Coral Reefs* 20: 399–408.
77. Delesalle B, Sourmia A (1992) Residence time of water and phytoplankton biomass in coral reef lagoons. *Cont Shelf Res* 12: 939–949.
78. Dumas F, Le Gendre R, Thomas Y, Andrefouet S (2012) Tidal flushing and wind driven circulation of the Ahe atoll lagoon (Tuamotu archipelago, French Polynesia) from *in situ* observations and numerical modelling. *Mar Pol Bull* 2012: 425–440.
79. Kraines SB, Suzuki A, Yanagi T, Isobe M, Guo X, et al. (1999) Rapid water exchange between the lagoon and the open ocean at Majuro Atoll due to wind, waves, and tide. *J Geophys Res* 104: 15,635–615,653.
80. Wiens HJ (1962) *Atoll Environment and Ecology*. New Haven: Yale University Press. 532 p.
81. Suzuki A, Kawahata H, Goto K (1997) Reef water CO₂ system and carbon cycle in the Majuro Atoll, the Marshall Islands in the central Pacific. *Panama Int Soc Reef Studies* pp. 971–976.
82. Suzuki A, Kawahata H, Ayukai T, Goto K (2001) The oceanic CO₂ system and carbon budget in the Great Barrier Reef, Australia. *Geophys Res Letters* 28: 1243–1246.
83. Andersson AJ, Gledhill DK (2012) Ocean acidification and coral reefs: Effects on breakdown, dissolution, and net ecosystem calcification. *Annu Rev Mar Sci* 5: 1.1–1.28.
84. Nugent LE (1946) Coral reefs in the Gilbert, Marshall, and Caroline Islands. *Bull Geol Soc Amer* 57: 735–780.
85. Charpy L, Rodier M, Fournier J, Langlade M-J, Gaertner-Mazouzi N (2012) Physical and chemical control of the phytoplankton of Ahe lagoon, French Polynesia. *Mar Pol Bull* 65: 471–477.
86. Andrefouet S, Payri C (2000) Scaling-up carbon and carbonate metabolism of coral reefs using in-situ data and remote sensing. *Coral Reefs* 19: 259–269.
87. Hochberg EJ, Atkinson MJ (2008) Coral reef benthic productivity based on optical absorbance and light-use efficiency. *Coral Reefs* 27: 49–59.
88. Kayanne H, Suzuki A, Saito H (1995) Diurnal changes in the partial pressure of carbon dioxide in coral reef water. *Science* 269: 214–216.
89. Ohde S, van Woessik R (1999) Carbon dioxide flux and metabolic processes of a coral reef, Okinawa. *Bull Mar Sci* 65: 559–576.
90. Smith SV, Marsh JA (1973) Organic carbon production on the windward reef flat of Eniwetok Atoll. *Limnol Oceanogr* 18: 953–961.
91. Qasim SZ, Bhattathiri PMA, Reddy CVG (1972) Primary production of an atoll in the Laccadives. *Internationale Revue der gesamten Hydrobiologie* 57: 207–225.
92. Kinsey DW (1972) Preliminary observations on community metabolism and primary productivity of the pseudo-atoll reef at One Tree Island, Great Barrier Reef. *Cochin, India*. pp. 13–32.
93. Kinsey DW (1977) Seasonality and zonation in coral reef productivity and calcification. *Miami, Florida. International Society for Reef Studies*. pp. 383–388.
94. Kinsey DW, Domm A (1974) Effects of fertilization on a coral reef environment - primary production studies. *Brisbane, Australia*. pp. 49–66.
95. Marsh JA (1974) Preliminary observations on the productivity of a Guam reef flat community. *Brisbane, Australia*. pp. 139–145.
96. Kinsey DW (1979) *Carbon turnover and accumulation by coral reefs* [PhD Dissertation]. Manoa: University of Hawaii. 248 p.
97. LIMER ET (1976) Metabolic processes of coral reef communities at Lizard Island, Queensland. *Search* 7: 463–468.
98. Atkinson MJ, Grigg RW (1984) Model of a coral reef ecosystem: II. Gross and Net benthic primary production at French Frigate Shoals, Hawaii. *Coral Reefs* 3: 13–22.
99. Barnes DJ, Devereux MJ (1984) Productivity and calcification on a coral reef: A survey using pH and oxygen electrodes. *J Exp Mar Biol Ecol* 79: 213–231.
100. Pichon M, Morrisey JI (1985) Premiers mesures de bilan metabolique dans l'ecosystem recifal de Tulcar (Madagascar). *CR Acad Sci Paris de la vie/Life Sciences* 300: 99–101.
101. Gattuso J-P, Pinchon M, Delesalle B, Canon C, Frankignoulle M (1996) Carbon fluxes in coral reefs. I. Lagrangian measurement of community metabolism and resulting air-sea CO₂ disequilibrium. *Mar Ecol Prog Ser* 145: 109–121.
102. Pichon M (1985) Organic production and calcification in some coral reefs of French Polynesia. *Tahiti, French Polynesia*. pp. 173–177.
103. Kraines S, Suzuki Y, Yamada K, Komiya H (1996) Separating biological and physical changes in dissolved oxygen concentration in a coral reef. *Limnol Oceanogr* 41: 1790–1799.
104. Mioche D, Cuet P (2000) Community metabolism on reef flats at La Reunion Island (Indian Ocean): natural versus anthropogenic disturbance. *Bali, Indonesia*. pp. 431–436.
105. Silverman J, Lazar B, Erez J (2007) Effect of aragonite saturation, temperature, and nutrients on the community calcification rate of a coral reef. *J Geophys Res* 112 (C05004).
106. Falter JL, Atkinson MJ, Merrifield MA (2004) Mass transfer limitation of nutrient uptake by a wave-dominated reef flat community. *Limnol Oceanogr* 49: 1820–1831.
107. Gattuso J-P, Pinchon M, Delasalle B, Frankignoulle M (1993) Community metabolism and air-sea CO₂ fluxes in a coral reef ecosystem (Moorea, French Polynesia). *Mar Ecol Prog Ser* 96: 259–267.
108. Symonds G, Black KP, Young IR (1995) Wave-driven flow over shallow reefs. *J Geophys Res* 100: 2639–2648.
109. Maragos JE (1978) Measurement of water volume transport for flow studies. In: Stoddart DR, Johannes RE, editors. *Coral Reefs: Research Methods*. Paris: UNESCO. pp. 353–360.
110. Young IR (1989) Wave transformations over coral reefs. *J Geophys Res* 94: 9779–9789.
111. Bonneton P, Lefebvre J-P, Bretel P, Ouillon S, Douillet P (2007) Tidal modulation of wave-setup and wave-induced currents on the Abore coral reef, New Caledonia. *J Coast Res* 50: 762–766.